12-2013

Thermal Analysis of Carbon Nanofiber Reinforced Isotactic Polypropylene

Anna Alicia Hernandez
University of Texas-Pan American

THERMAL ANALYSIS OF CARBON NANOFIBER REINFORCED ISOTACTIC POLYPROPYLENE

A Thesis

by

ANNA ALICIA HERNANDEZ

Submitted to the Graduate School of
The University of Texas-Pan American
In partial fulfillment of the requirements for the degree of

MASTER OF SCIENCE

December 2013

Major Subject: Mechanical Engineering

THERMAL ANALYSIS OF CARBON NANOFIBER REINFORCED ISOTACTIC POLYPROPYLENE

A Thesis
by
ANNA ALICIA HERNANDEZ

COMMITTEE MEMBERS

Dr. Karen Lozano
Chair of Committee

Dr. Magdalena Chipara
Committee Member

Dr. Dorina Mihut
Committee Member

Dr. Mircea Chipara
Committee Member

December 2013

ABSTRACT

Hernandez, Anna A., Thermal Analysis of Carbon Nanofiber Reinforced Isotactic Polypropylene. Master of Science (MS), December, 2013, 71 pages, 2 tables, 51 figures, references, 39 titles.

Isotactic Polypropylene (IPP) is a commonly known thermoplastic that has unique properties include being light weight, high performance, impact strength, tensile strength, elongation, and high temperature properties. The use of vapor grown carbon nanofiber (VGCNF) reinforcements on polypropylene has shown to produce high specific modulus, strength, electrical and thermal properties on specimens. Thermogravimetric (TGA) investigations on the thermal degradation of isotactic polypropylene – vapor grown carbon nanofibers composites in nitrogen were reported. The mass evolution as a function of temperature is a single sigmoid for both polypropylene and polypropylene loaded with VGCNF. The inflection temperature of these sigmoids increases as the concentration of VGCNF is increased. The width of the degradation process narrows as the concentration of VGCNF is increased due to a better homogenization of the local temperature provided by the high thermal conductivity of carbon nanofibers. TGA analysis data indicates the formation of polymer – VGCNF interface.

DEDICATION

I would first like to thank God for giving me the knowledge, strength, and determination to complete a significant aspect of my life. I would like to dedicate the completion of my masters' studies to my family and friends, who without their support and encouragement would not have been possible.

ACKNOWLEDGMENTS

I would like to express my deepest gratitude to Dr. Karen Lozano, my thesis advisor, for her patient guidance, enthusiastic encouragement and useful critiques of this research work. My thanks to my thesis committee members: Dr. Magdalena Chipara, Dr. Dorina Mihut, and Dr. Mircea Chipara. Their advice, input, and comments on my thesis helped to ensure the quality of my intellectual work.

I wish to express my thanks to all members of the Nanoteam for their support, help, and friendship. I extend my appreciation and thanks to the technicians of the laboratory of the Mechanical Engineering Department for their help in offering me the resources.

This thesis would be incomplete without the mentioning of the support that was given by my family and friends. A special thanks to Veronica Hernandez, Norma Hernandez, Carina Olvera, Laura Martinez, and Veronika Villa for their constant encouragement. My great appreciation goes to Ruben Gutierrez Jr., who was always there to give his best advice and stood by me through the good times and bad. I want to thank my parents who taught me that hard work and dedication would make nothing impossible.

Last but not least, this research was supported by the National Science Foundation under account number #A2-1299.

TABLE OF CONTENTS

Page

LIST OF TABLES

LIST OF FIGURES

CHAPTER I

INTRODUCTION

Polymers are becoming one of today's industries primary materials for the manufacturing of parts and components that were once made by wood, metal, ceramic, or glass. They are often being referred to as plastics because most commercial polymers are enhanced with additives. Their unique properties include being light weight, high performance, impact strength, tensile strength, elongation, and high temperature properties. Polymers are divided into two categories – thermosets and thermoplastics. Thermosets (TS) are a type of plastic that has undergone a chemical reaction and cannot be reversed. As a result, once it has been molded, it cannot be reshaped under heat and pressure. Examples of TS are epoxy, melamine, phenolics, and unsaturated polyester. Thermoplastics (TP), on the other hand, are materials that when solidified and reheated will be able to flow once again and allows the plastic to be reshaped. In addition, TP are divided into amorphous and semi crystalline polymers. TS can only be amorphous polymers. The two most popular TP polymers are polypropylene and polyethylene because they are built from two monomers that are of great interest.

The figure below shows the amorphous (A) and semicrystalline (SC) regions, they describe the morphology of polymers in their solid state. For A, the molecules in the polymer are oriented randomly and intertwine with each other; it is often described like spaghetti when cooked. The polymer in this state has a transparent appearance like glass. In contrast, the molecules in SC polymers are packed together in regions called crystallites. When the polymer is above the melting temperature of the crystals, the polymer exists as a viscous liquid. When the crystals are cooled, they nucleate and grow to fill the volume that is vacant. Also, polymers are referred to as semicrystalline because some of the regions remain uncrystallized or amorphous when cooled to room temperature. This is because the crystals begin to grow and trap the amorphous region within, restricting any type of movement. [1]

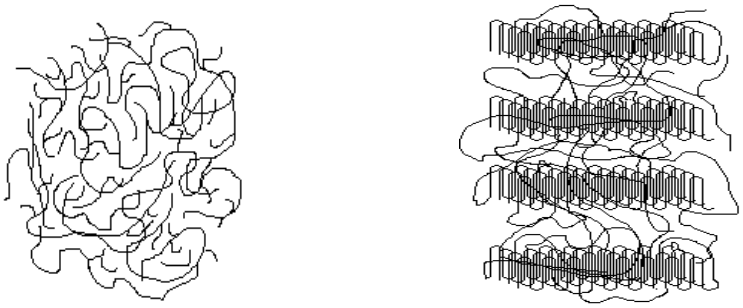

a. Amorphous b. Semicrystalline

Figure 1: Amorphous and Semicrystalline polymer regions

Presently, there are many new manufacturing techniques that are being used to improve the material's properties of polymers. The use of carbon nanotubes (CNT) and nanofibers (CNF) as reinforcements in polymers is being widely explored. It is of great interest because the properties of the material are becoming size dependent at low dimensions. Theoretical predictions and experimental observations have also shown that they produce high specific

modulus, strength, electrical and thermal properties on specimens. [2-5] Recent studies revealed that the polymer's properties are being influenced by the processing parameters and the CNT/CNF present in the matrix. [6-12] This has led to a considerable interest in the fabrication of polymer nanocomposite. The morphology of these materials is being examined by static and dynamic testing.

1.1 Isotactic Polypropylene (IPP)

IPP is one of the most studied polymers because its structure and properties are commonly known. It is identified as a thermoplastic that has a higher consumption because of it physical and mechanical properties. Also, this polymer is easy to process with a relative low cost, making it a resourceful material. The word isotactic is the tacticity of the polymer and refers to the formation of the branched monomers. The branch groups are all on the same side of the polymeric chain and are arranged in the same geometric pattern. The figure below shows the chemical structure of IPP.

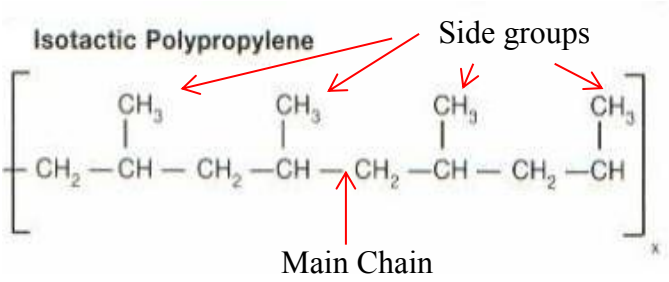

Figure 2: Chemical Structure of IPP

In crystalline polymers, the morphology and microstructure contain important information about the history of the polymer. The degree of crystallinity helps define the polymer but it also dependent on the way the lamellae is organized (spherulitic structure). [13] Spherulites growth is not caused by additives but is produced when there is molecular folding. [14] There are many

methods that are being used to understand the kinetics of polymer crystallization in order to relate it to nucleation, spherulite growth, and crystallization rate. [15-16]

Thermal conditions, mechanical effects, and the presence of additives in polymers influence the characteristics of the supremolecular configuration. During the crystallization stage, various supermolecular structures form as aggregates of chain-folded fibrillar or lamellar primary crystallites with definite geometrical arrangements. When polymers crystallize in a melt, different supermolecular formations may develop, most frequently spherulites and cylindrites (axialites), with some hedrites (polygonal formations), quadrites (tetragonal formations), and dendrites (pine-shaped formations). Although, the two main morphological identities present from a melt are spherulites and lamellae. [17]

IPP when crystallized by a melt will adopt a 3_1 helical confirmation with chain axis that repeats at a distance of 6.5 Å. The three-fold helix indicates that it takes three monomer units to make one helical turn. IPP crystallizes into three phases: monoclinic α-phase, pseudo-hexagonal β-phase, and a trigonal or orthorhombic γ-phase. Each phase will form at certain crystallization conditions. [18]

In 1960, the α-phase was discovered by Natta and Corradini. It is the most common crystal present in IPP with overall parameters of the cell being a = 6.65 Å, b = 20.96 Å, c= 6.5 Å, β = 99.8°. The lamellar branching that occurs is extraordinary to polymer crystallography and to the crystal form itself. This type of branching happens in every crystallization condition such as in solution crystallization, thin film growth, spherulitic growth, and fibers. Although at very high (>160 C) or low (<~90 C) temperatures the lamellar branching will decrease. The monoclinic

phase of IPP is a very important molecular marker because it defines the structure and no other crystalline polymer is the same.

The β-phase of IPP is metastable and usually occurs under a temperature gradient, shear, or in the presence of specific β nucleators. [19-21] The β phase depends on the concentration of additives and on the cooling conditions that occur during the melt crystallization. The β-phase usually occurs within a temperature of T≈155C and will grow 70% faster than α-phase if the temperature range is from 141 C to 105 C. If it is outside this range, the α-phase will grow faster. Also, the β phase has a higher melting temperature and density compared to the α-phase. This is why the β phase has strong differences in mechanical properties like having higher toughness and drawability but is lower in stiffness and strength. [22] The parameters had remained a mystery until Turner-Jones and Cobbold suggested a hexagonal unit cell with parameters of a=b= 19 Å, c=6.5 Å. It was not until 1994, Meille and Lotz (independently) got the same solution of a trigonal cell that had three isochiral helices with parameters of a=b= 11.01 Å, c = 6.5 Å. This phase is often described as being "frustrated" because it does not follow "classical" crystallography. [23-24]

The γ- phase has been undefinable for many years because it is not observed as a different phase but usually crystallizes with and within the α-phase spherulites. In 1961, Addink and Beintema found the γ- phase using X-ray patterns from low molecular weight IPP. In 1989, Meille and Brickner suggested that it was a triclinic cell with a subcell of a larger face centered orthorhombic unit with parameters of a = 8.54 Å, b=9.93 Å, and c = 42.21 Å. Although, there are no fiber patterns that are available and electron micrscopes have shown that it occurs in the ac

face of the α phase of IPP. Many studies have shown that the γ formation is likely to occur in degraded PP, low molecular weight PP or under high pressure crystallization. [18]

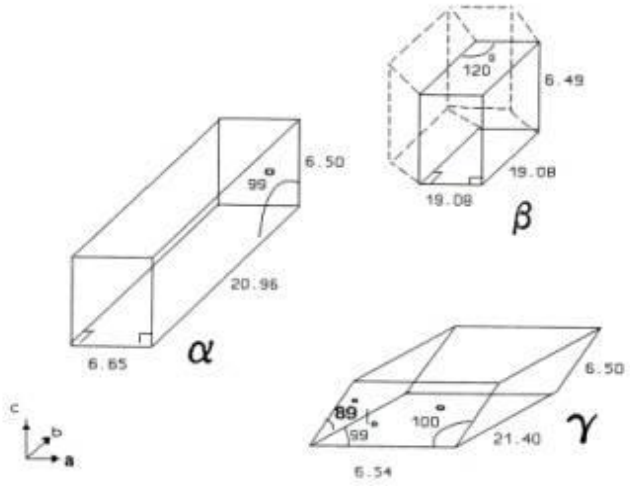

Figure 3: Crystallization Phases of IPP

Much investigation has been done on IPP and the impact carbon nanofibers will have on it. The PP with CNF composites matrix have been greatly influenced by the addition of fibers that act as nucleant agents. This means that the crystalline morphology of the polymer has been affected because the fibers manipulate the crystallization process.

1.2 Carbon Nanotubes/Nanofibers (CNTs/CNFs)

In 1985, fullerenes were discovered at Rice University by Robert Curl, Richard Smalley, and Sussex Professor Harold Kroto. Fullerenes are molecules composed entirely of carbon and its third allotrope. They are in the form of a hollow sphere, ellipsoid, tube, or plane. The spherical fullerenes are also called buckyballs, and cylindrical ones are called carbon nanotubes or buckytubes and were observed in 1991 by Sumio Iijima. They can be divided into two

categories single walled nanotubes (SWNT) and multi-walled nanotubes (MWNT). SWNT consist of a single "rolled-up" layer of graphite comprising carbon hexagons and MWNT are made up of many concentric cylinders. [25-26] Many papers have focused to characterize the CNT in order to find out its structure, properties, and the potential applications. [27-28] One study showed that the carbon –carbon sp2 bond is responsible the high strength and modulus of a CNT. This means that the structure is dependent highly on the strength between the interatomic bonds. [29] There are different methods to manufacture CNT/CNF. The three most common are arc discharge synthesis, pyrolysis of carbon atoms, and laser evaporation of graphite. [30] Each method used will give you a variation between what type of CNT/CNF you will have. For example, in the arc discharge method, MWNTs are more likely to be produced that SWNTs. Vapor grown carbon nanofibers (VGCNFs) are a special class of CNFs because of the method they are produced. They are created from a gas phase decomposition of a hydrocarbon in the presence of a catalyst. The graphite networks are arranged in concentric cylinders with carbon layers arranged like tree rings forming

The use of VGCNF – reinforced composites is of great interest because of their extraordinary properties. The impact of using carbon nanofibers reinforcements on polypropylene has shown to produce high specific modulus, strength, electrical and thermal properties on specimens. VGCNF are special class of carbon nanofibers because of the method they are produced which give them exceptional physical characteristic and low cost fabrication. They are produced by using a metal catalyst particle, such as iron, and are exposed at a very high temperature gas supersaturated in carbon. The catalyst particles are then carbon fibers that are in nanometer diameter and are approximately around the range of 200 nm. The investigation of polypropylene-carbon nanofiber composites was done in order to understand the processing and

thermal behavior between the mixtures. Previous studies have shown that good quality samples are achieved by permeation of the fibers and the matrix. [31] This improves the nanofiber/matrix wetting plus an exceptional bond. Although this has not been the case for all polymers, specifically glassy polymers such as epoxy and poly (methyl methacrylate) showed only moderate enhancement or a slight decline in the modulus and strength and this usually cause by the nanotubes incorporation. Several issues that are well known to affect to the reinforcements are the dispersion state, filler-matrix interfacial property, and nanotube alignment in polymers.

1.3 Composite Analysis

There is a range of methods that currently being used for the characterization of IPP to determine the material's property. The types of techniques that have been used for thermal investigation are as followed: Thermogravimetric Analysis (TGA), Differential Scanning Calorimetry (DSC), Dynamic Mechanical Analyzer (DMA), and Scanning Electron Microscopy (SEM). The physicochemical properties of reinforced polypropylene composites have been investigated on single walled, multi walled nanotubes, and vapor grown carbon nanofibers.

TGA is a thermal analysis technique used to measure the change of weight of a material as a function of temperature and time. It is used to determine a material's thermal stability and its fraction of volatile components by monitoring the weight change that occurs as a specimen is heated. Typical heating rates employed in TGA measurements of carbon nanotube specimens are in the 10-20 C/min range. Although in literature it was reported that heating rates were as high as 100 C/min and as low as 1 C/min. It has also been reported that the heating rate has a profound effect on the measured values. The TGA was used to evaluate the thermal stability of 0.5 wt. % CNF reinforced powered PP. Tests were conducted at a heat rate of 10 C/min from ambient to

600 C under nitrogen gas atmosphere. It clearly stated that the CNF/PP composite was more thermally stable than PP by itself. [34]

In general the presence of carbon nanotubes (CNT) in polymers has shown to increase the mechanical properties and glass transition temperature. The crystallinity has the most influence on the mechanical properties' modulus and toughness since most failure has occurred in composites at the microscopic level. [33] DSC uses a quantitative method to find the degree of crystallinity that the sample may have and is usually used to measure the glass transition temperature. It is used to determine the temperature and heat flow associated with material transitions as a function of time and temperature and to characterize melting, crystallization, resin curing, loss of solvents, and other processes involving an energy change. A recent study showed that the crystallization characteristics such as crystallinity, spherullite size and structure influenced IPP. It was seen the degree of crystallinity was altered by 1 vol. % MWNTs and also increased the crystallization temperature by 13C. [37] The nonisothermal crystallization behavior of single walled nanotubes (SWNT) reinforced on IPP was studied. It was indicated that the PP crystallization was reduced as the addition of low SWNT percentage. An assumption was made that the PP crystals were affected by the SWNT because they behaved as nucleating agents in the composite even at a low percentage. [36-37] The nanotubes have shown to have a positive effect on the crystallization kinetics of PP. Also, the decrease of enthalpy with increasing nanotubes concentration happened because the PP concentration in the composite has decreased. There has been no significant change in the melting point of polypropylene phase.

DMA and Dynamical Mechanical Thermal Analysis (DMTA) are analyzers used to study and characterize material. The DMA and DMTA measures the mechanical properties of materials as a function of time, temperature, and frequency. If is frequently used for observing

the viscoelastic nature of polymers. The two common methods currently used are the decay of free oscillations and the other is forced oscillation. Free oscillation techniques involve applying a force to a sample and allowing it to oscillate after the force is removed. Forced oscillations involve the continuing application of a force to the sample. An oscillating force is applied to a sample of material and the resulting displacement of the sample is measured. DMTA showed that the polymer was greatly enhanced with longer MWNT than short ones. This could be because the load transfer between two phases was favored by long fibers which lead to better stiffness of the composite. It was shown that the effect of the stiffness was greatly influenced at a lower temperature. [37]

Scanning Electron Microscopy (SEM) analysis has been done to find information of the composites at the micro/nano scale. The SEM uses a focused beam of high-energy electrons to generate a variety of signals at the surface of solid specimen. The signals contain information about the sample's surface topography, composition and other properties like electrical conductivity. The SEM is used for analyzing CNT/CNF because it can produce images that may be magnified to show features down to the nanometer scale. Also, chemical information may be acquired from areas measuring several square millimeters, all the way down to one micrometer for thick samples and less than 50 nm for thin samples. With the addition of a detector, it is capable of analyzing uncoated samples and able to uncover nearly all length scales from TEM to light microscopy. [32]

Although many studies have been done on the analysis of polypropylene and CNT/CNF composites, there is still not a clear understanding on the fabrication methodologies, processing parameters, morphology characterization, and fundamental physics. There is still a big gap that needs to be filled to understanding the thermal stability of CNT/PP composites.

CHAPTER II

EXPERIMENTAL INSTRUMENTATION

In this chapter, the experimental instrumentation that was used to obtain and analyze the nano reinforced polymer composites will be discussed. The chapter will include an explanation of the basic principles underlying the techniques and will include schematics of the instruments.

2.1 HAAKE PolyLab System

The Polylab Haake Rheomix was used as the main source for mixing and incorporation of the matrix and reinforcements in the melt. The extensive shearing and elongation flows contributed to a positive dispersion and distribution of the reinforcement phase within the matrix. This machine is able to disperse the solid agglomerate within thermoplastics matrices in the melt phase. The mixer sensor produces a graph of the dynamic viscosity that depends on shear load, melt behavior, influence of additives, temperature, and shear load behavior. Dispersion has been found to be a key factor that influences composites and it is dependent on the mixing parameters such as: mixing time, rotor speed, rotor blade geometry, and temperature. The mixer can be defined as a Banbury type mixer and has two rotors that rotate in opposite directions with a 3:2 (drive: driven) gear ration as shown in Figure 4.

Figure 4: Polylab Haake Rheomix

This rotating action and blade configuration provides shear forces capable of breaking the agglomerates. The mixer consists of three plates that have thermocouples attached to each one to control temperature as the material is being mixed. The driving unit technical specifications for the PolyLab Rheochord 300p is listed in Table 1.

Motor Power	7.5 kW
Speed Range	2 - 200 min^{-1}
Torque Range	0 - 300 Nm
Temperature	450^{0} C

Table 1: Technical specification for Polylab Haake Rheomix

2.2 Haake MiniLab

The Haake MiniLab is a mixing instrument that is based on a conical twin-screw compounder with an integrated backflow channel as shown in Figure 5. It is used to compound and extrude small amounts of the material of no more than 7 grams.

Figure 5: HAAKE MiniLab

The backflow channel and integrated pass valve enables the recirculation of the melt. The residence time, the amount of substance present by the flow rate in the system, can be monitored. There are two pressure transducers that are measuring the viscosity of the melt. Table 2 is showing the technical specifications for the system.

Motor Power	0.4 kW
Speed Range	10 - 360 min^{-1}
Torque Range	0 - 5 Nm
Max Temperature	350^{0} C

Table 2: Technical Specifications for the HAAKE MiniLab

2.3 Carver Heated Platens

The Carver Heated Platens (Hot Plates), Figure 6, were used to mold the matrix together; it is capable to process at temperatures up to 650 F. The platens are controlled and include a mechanical thermoset on each individual platen. The platens were equipped and cored for cooling water.

Figure 6: Carver Heated Platens

2.4 Universal Testing System

A Universal Testing System (UTS), Figure 7, was utilized to determine the tensile properties of the polymer and composites. The mechanical testing system (MTS) Sintech was used to perform the tensile testing. Tensile testing methods are used to measure the force required to break a specimen and the extent to which the specimen stretches or elongates to that breaking point.

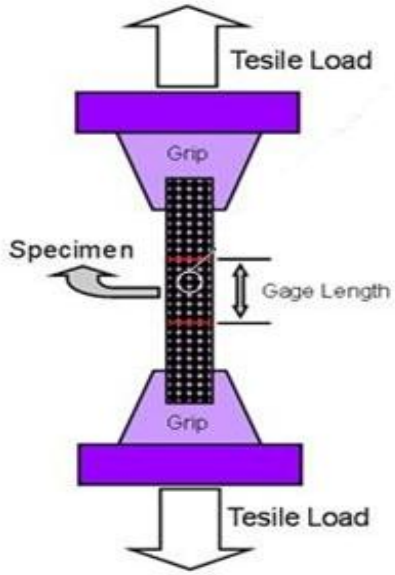

Figure 7: Tensile Testing Schematic

The MTS (Figure 8) has the capability to calculate the modulus, strain at break, peak stress, and peak load. The MTS components include the test frame, analysis software, test fixtures, and devices used to hold and support the specimen. As the sample is tested the measurements are taken by the load cells and extensometers.

Figure 8: MTS Sintech 65/G

2.5 Thermogravimetric Analysis – TGA

Thermogravimetric Analysis is used to measure the weight changes (degradation) of a material that occurs with temperature. It is primarily used to determine the thermal stability or degradation of a sample though analysis of sample composition is also possible; samples can be fingerprinted as consisting of a homopolymer, copolymer, or composite materials. Elemental analysis is also possible when coupled with a mass spectrometer or Fourier Transform Infrared Analyzer. The amount and rate of change in the weight of a material can be taken as a function of temperature or time in a controlled atmosphere. The transformation of the material from thermodynamic state to another is detected by decomposition, oxidation, or dehydration. The information obtained is used to identify the percentage of weight change according to the chemical structure, process, and end performance.

Figure 9: TGA Q500

The thermogravimetric analyzer (Figure 9) consists of six major components: the balance, sample platform, furnace, cabinet, heat exchanger, and two mass flow controllers. A sample is placed in a pan that is then enclosed into a furnace. The furnace controls the sample

atmosphere and temperature. It will heat the sample while the balance will continuously measure the weight until complete degradation.

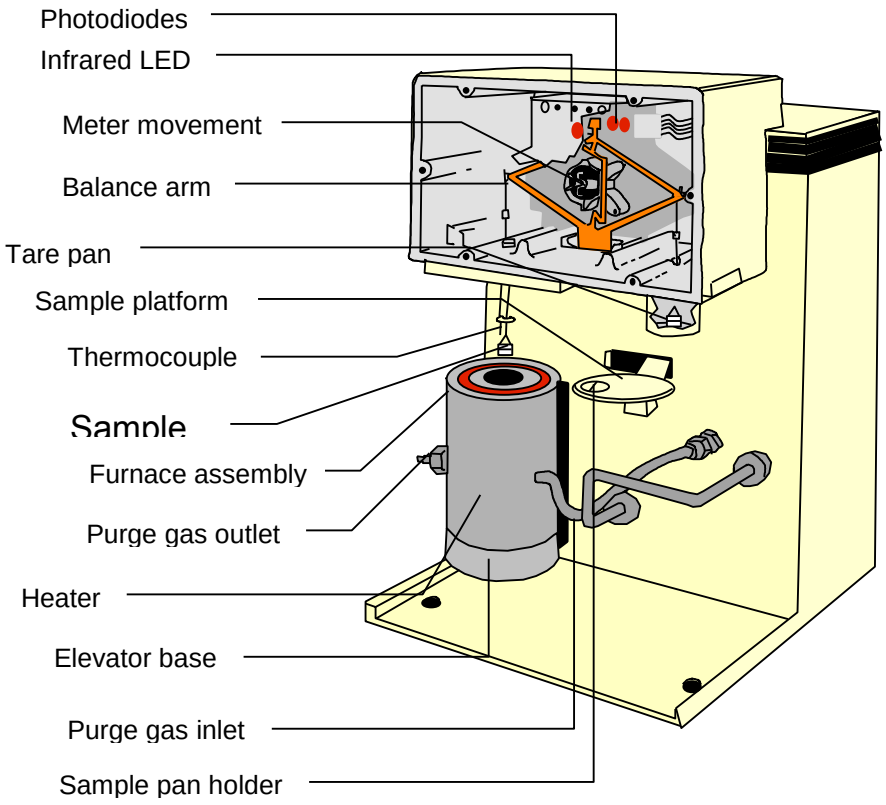

Figure 10: TGA Schematic

2.6 Differential Scanning Caliometry – DSC

Differential Scanning Caliometery is used to determine the heat flow as a function of time and temperature in materials. It provides information about phase changes such as amorphous and crystalline transition and chemical changes such as in sample degradation or reactions within the sample. In other words, it is used to characterize melting, crystallization, glass transition temperature, percentage of crystallinity, resin curing, loss of solvents, and other processes involving any type of energy change.

Figure 11: DSC Q100

The three major components of the DSC (Figure 11) are the instrument itself, the cell, and the cooling accessory. The cell and accessory play a major part. The cell monitors the heat flow and temperature and the accessories can be used when needed for the experiment.

Figure 12 shows the schematic of the DSC.

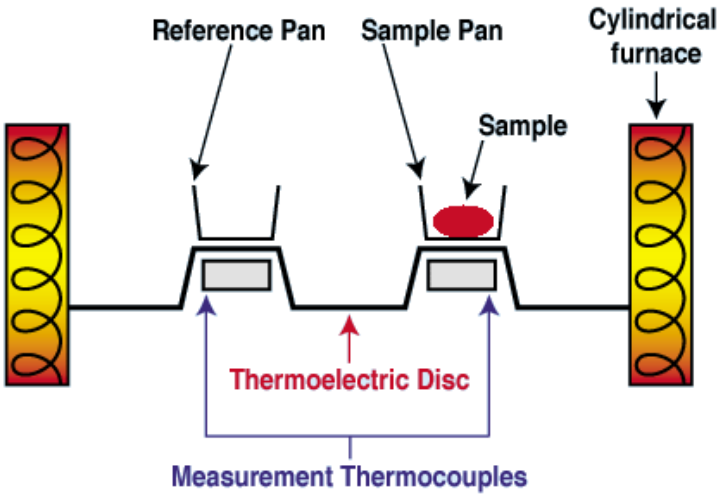

Figure 12: DSC Schematic

It is a heat –flux DSC system since both the sample and reference were enclosed in the same furnace. A metallic block with high thermal conductivity was placed between both the sample and reference in order to maintain a consistent heat flow path. The DSC is a technique that relies on the differences in energy required to maintain both the sample and the reference at

identical temperature. The enthalpy or heat capacity changes in the sample compared to the temperature differences relative to the reference. The temperature difference is then recorded between both the sample and the reference. In order to ensure the measurements are maintained constant throughout the experiment, it should be performed under a vacuum or inert-gas flow.

2.7 Transmission Electron Microscope – TEM

The TEM is an instrument in which an electron beam is focused on the specimen and images are formed by the transmitting of the electron beam in a way of geometrical optics. Since electron beam wavelengths are short, TEM can obtain high magnification and high resolution image. High energy (>100 kV) electrons and electromagnetic lenses are used. The electron beam passes through an electron transparent sample and by using the lenses an image is formed and projected onto a fluorescent screen or a CCD camera. The image contrasts are formed by the intensity of scattering of the electrons at each part of the specimen. Resolution of recent TEM reaches 0.2 nm to 0.3 nm, which is close to the theoretical resolution. Different contrasts are produced from the scattering of crystal planes. This means that the contrast depends on the orientation of a crystalline area in a sample. The TEM has a high resolution that allows for the atomic arrangements to be enlarged in detail. The main components of a TEM are shown in Figure 13: the electron beam, the condenser system, the sample, the image formation, projection of image (magnification), and the recording of the image.

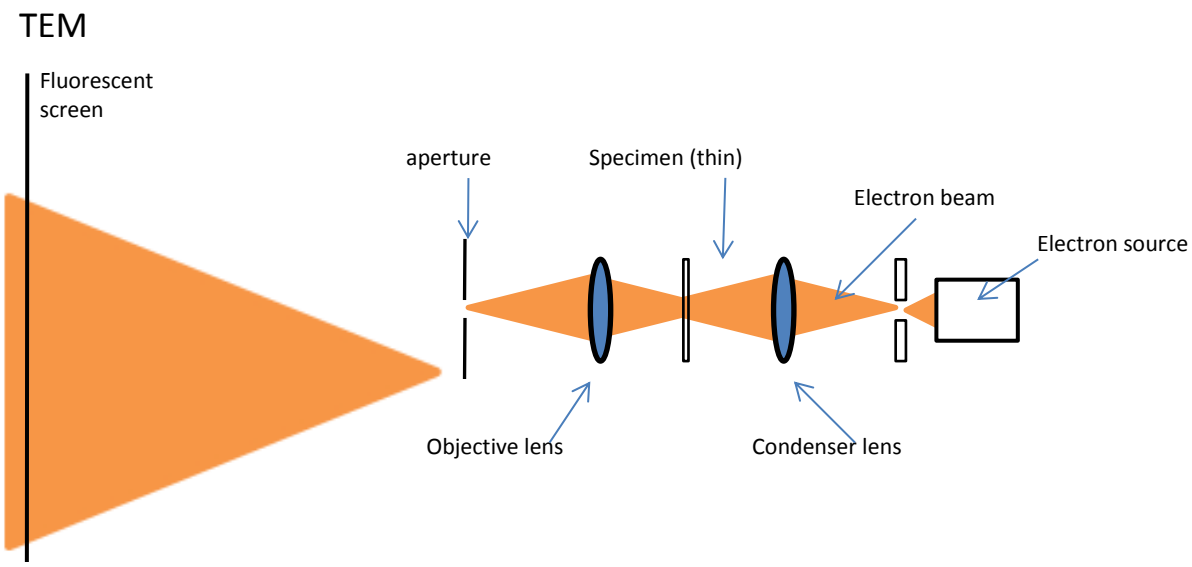

Figure 13: TEM Schematic

CHAPTER III

EXPERIMENTAL PROCEDURES

In this chapter, the experimental procedures performed on the VGCNF reinforced isotactic polypropylene will be discussed. The procedure was based on previous research that was performed on VGCNF reinforced high density polyethylene (HDPE). Previous results revealed that increased shear history increased the work of fracture and allowed for better dispersion of the nanoreinforcements, improved infiltration of the matrix, and stronger matrix-reinforcement interface. Several studies were conducted to understand how processing parameters were influencing the improved properties. A better understanding of the thermal history caused by the shear action was needed besides the fact that the available literature on carbon nanofiber reinforced polypropylene composites and its processing effects was not widely available thus a greater interest developed for this project. A systematic study of the effect of shear force during mixing of VGCNF reinforced isotactic polypropylene on the ultimate properties was conducted. An isotactic polymer was used to avoid adding extra variables present on atactic systems. The objective of this research was to study the effects of mixing parameters such as temperature, speed, and time on VGCNF reinforced isotactic polypropylene (IPP) and perform static and dynamic testing in order to understanding the morphology of the composite

The materials that were used for the fabrication of the functionally graded materials were isotactic polypropylene (IPP) and vapor grown carbon- nanofibers (VGCNFS) reinforced polypropylene composites.

3.1 Isotactic Polypropylene

The material used in the study was IPP type Marlex HLN-120-01 manufactured by Philips Sumika Polypropylene Company. The density is 0.906 g/ cm^3 and has a melt flow rate at 230° C of 12 g/ 10 min. IPP was processed by using an injection and compression molding techniques. The purpose of the IPP was to hold the nanofibers together due to the fact that the nanofibers alone are brittle and the matrix adds toughness to the composite.

3.2 Vapor Grown Carbon Nanofibers (VGCNFs)

The VGCNFs labeled PR-24-AG (Pyrograf products) were provided by Applied Science Inc. Their diameters range between 60 and 100 nm with the lengths ranging between 30,000 and 100,000 nm.

3.3 Purification of VGCNFs

The purification process as developed by Lozano et al. [39] consisted of refluxing a suspension of VGCNFs and dichloromethane. A transformer was set at 140 Volts, at 35°C and under stirring with a magnetic stirrer. The VGNF were left for 5 days in this state while checking the flux. After the 5 days, the fibers were washed using deionized water. Then, the VGCNF were left to reflux in deionized water for 2 days at 140 Volts, 90°C and under stirring conditions. After 2 days, the fibers were washed again with deionized water. The VGCNFs were left under

the vacuum for 4 hours covered with a parafilm. The fibers were placed in a beaker and covered with aluminum paper and baked at 108°C. This would allow for the water to evaporate. They were left in the oven for 2 days (one day under vacuum). Finally after 2 days, the beaker was taken out to be cooled down and was then used to create the composite.

3.4 Composite Preparation

Different percentages of CNF were used as reinforcements for isotactic polypropylene. In this study the VGCNF were mixed with IPP using the HAAKE Rheomix. Samples of +/-35 grams with different VGCNF concentrations were prepared. The prepared samples had 0, 1, 2.5, 5, 7.5, 10, 15, and 20wt% of VGCNFs. The first mixing was conducted at a temperature of 180° C (350°F) with a mixing speed of 65 rpm for 9 min and 90 rpm for 5min. The samples were pressed into films of a thickness of ≈ 0.025 in on a heated press at ≈180°C for 1 ½ minute. The films were then pelletized into squares ≈1/8 inch x 1/8 inch. Once pelletized, the composites were exposed to higher shear forces of 100 rpm for 3 min and 100 rpm for 10 min using the Thermo HAAKE MiniLab system which is capable of mixing +/- 4.5 grams. The composite was pressed once more before testing. This processed was repeated for temperatures of 150° C, 165°C, and 195°C. This was done in order to make a comparison of the effect between the temperatures and the effects that it has on the composites.

The dynamic analyses were performed using: Mechanical Testing, TGA, and DSC while static analysis consisted of TEM.

3.5 Mechanical Testing

Mechanical testing was performed for each sample to compare the results that were obtained from the high density polyethylene material. The mechanical properties of the samples were investigated using the MTS Sintech 65/G. One of the important aspects was to analyze the sample and the resistance in breaking under tensile stress with the addition of more shear stress. The tensile specimens were prepared according to the ASTM D882-02 standards. The speed of testing was set at 50.8 mm/min with an initial gap of separation of 50.8 mm. The standard required the films to be less than 1 mm (0.039") in thickness with a width between 0.2 inch and 1.0 inch and length to be between 4.0 and 10 inches. The samples were cut with a die with the dimensions of 4" x 0.5" with a 0.025" thickness. The increase of CNF %, temperature, time, and speed affected the samples.

3.6 TGA

The Thermogravimetric Analysis (TGA) measures the amount and rate of change in the weight of a material as a function of temperature or time in a controlled atmosphere. The measurements are used primarily to determine the composition of materials and to predict their thermal stability at temperatures up to 1000°C. The sample was put under nonisothermal conditions; the thermal stability of the sample was performed in a nitrogen atmosphere. The samples weighing 10.0 ± 1.5 mg were heated to 1000 ºC at a rate of 20 ºC/min.

3.7 DSC

The DSC was used to determine the temperature and heat flow associated with material transitions as a function of time and temperature. It was used to characterize the melting,

crystallization, resin curing, loss of solvents, and other processes involving an energy change. The DSC was held under isothermal crystallization using the following conditions: it was equilibrated to 40 °C and ramped to 10 °C/min to 180 °C; it was then left at isothermal for 10 minutes, then ramped to 40°C/min to 140 °C and left isothermal for 200 minutes. The final ramp was 10ºC/min to 40 °C. The sample was set at isothermal temperatures of 135 °C, 137.5 °C, 142.5 °C, and 145 °C with each sample weighing about 10.0 ± 1.5 mg. Following the same procedure, the samples were then tested again but instead of using 40 °C /min it were changed to 50 °C /min and the temperature of 190 °C was changed to the melting temperature.

The data was then graphed and analyzed in order to determine the dispersion and interface that was developed from the increase of shearing.

CHAPTER IV

RESULTS AND DISCUSSIONS

In this chapter, the results obtained from the experiments done using the mechanical and thermal testing were evaluated. The last section continues with a discussion of the Avrami equation that was used to interpolate the data obtained.

4.1 Mechanical Testing

The mechanical properties of the samples will be discussed in relation of the increase with the concentration of CNF in IPP. At a temperature of 150 °C, the samples required high torque for mixing and were very stiff when removed from the HAAKE Rheomix; they had to be reheated to 160 ºC for a complete melt. The samples were then mixed at a temperature of 165°C, at this temperature, the samples were at an incomplete melt and the when pressed the sheets contained many voids. When the temperature was increased to 195°C the sample degraded and produced brittle sheets. At a final temperature of 180 ºC, the samples melted without degradation and a better mixture was produced. Also, when pressed the sheets contained little to no voids.

Figure 14 shows the results that were obtained using the MTS Sintech Testing equipment for the 180 ºC samples. The first mixing parameters were evaluated since they produced a better dispersion sample. It can be seen as the concentration of CNF % increases, the strain increases as well.

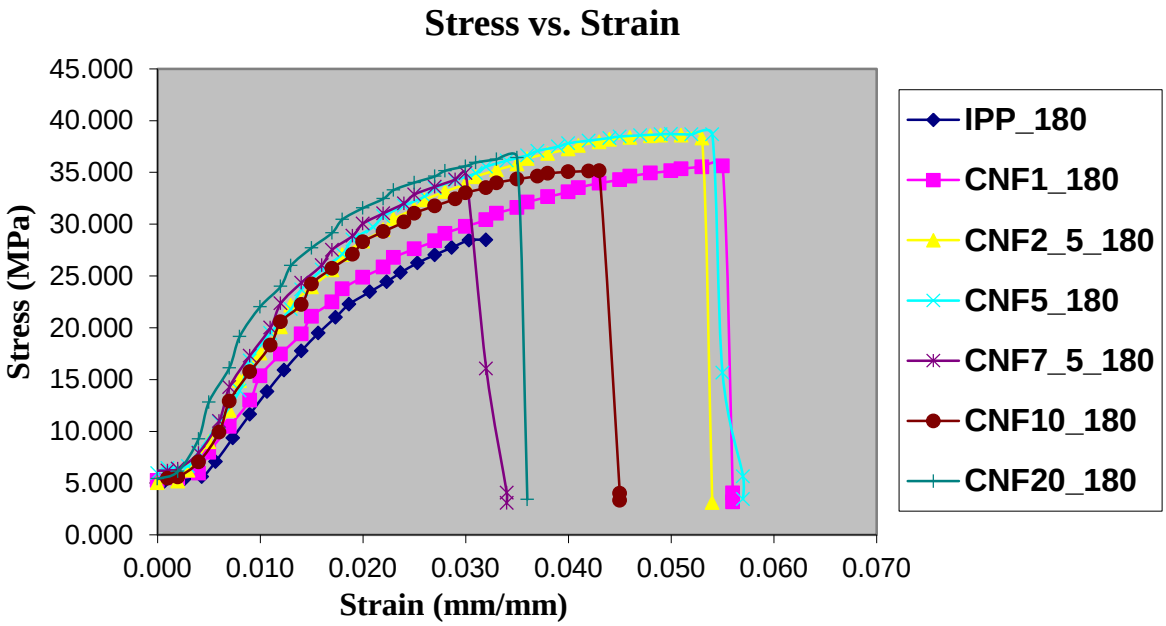

Figure 14: Strain vs. Strain for samples at T = 180 ºC, 65 rpm – 9min, 90 rpm – 5 min

The samples were then mixed with an additional mixing time using the HAAKE MiniLab at 100 rpm for 10 minutes. In Figure 15, the addition of CNF increases, the strain (the extensibility) of the material also increases for the pure polypropylene by itself.

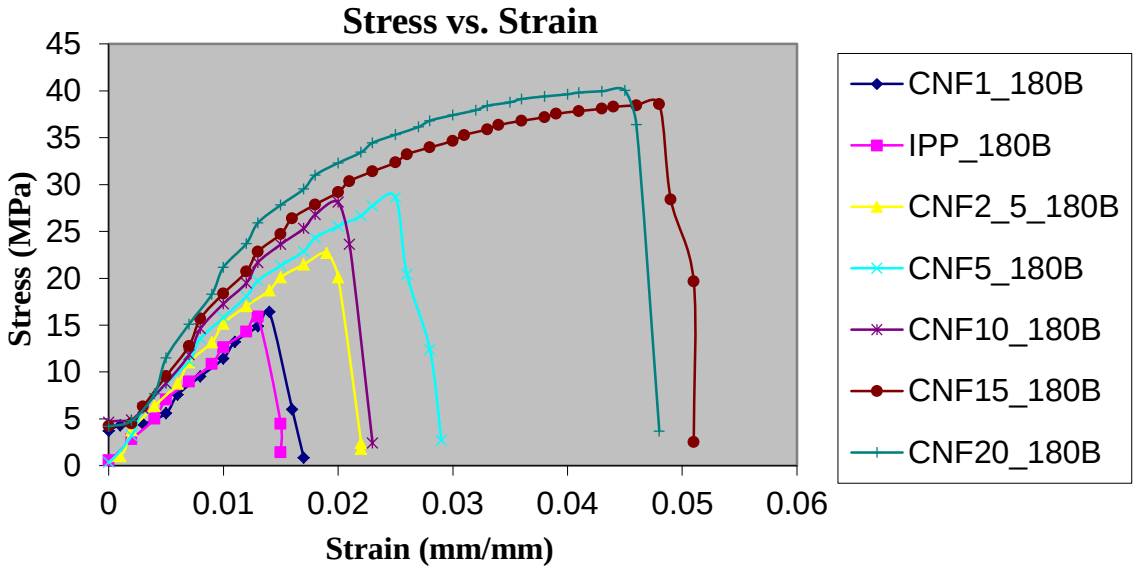

Figure 15: T=180 C, 1st Mix plus 2nd Mix: 100 rpm - 10 min

Figure 14 and 15 compares the samples with the first mixing and second mixing parameters. The first mixing parameters were taken into consideration due to the fact that a better mixture was created because of the extensibility of the material. In Figure 16, the strain at break versus the increase of concentration CNF (%) is shown. For pure polypropylene the strain of break increases as CNF is added; it is the highest at 2.5 % and 5% but later decreases with the increase of CNF.

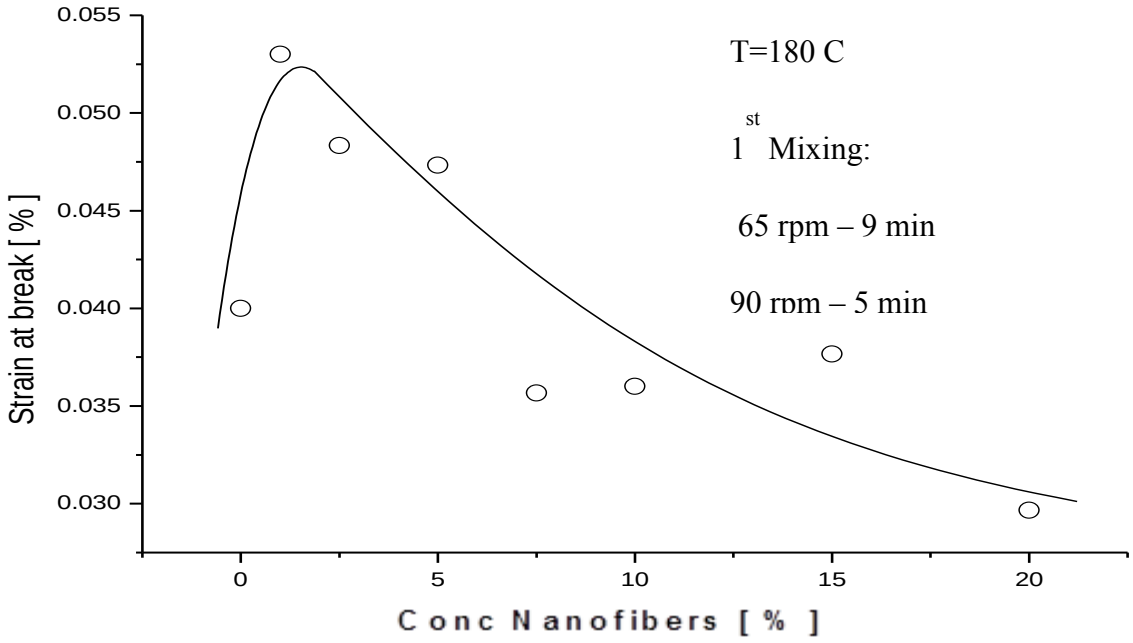

Figure 16: Strain at break vs. Concentration of Carbon Nanofiber %

The Young Modulus versus the CNF percentage, Figure 17, shows the modulus increased with the increase of CNF percentage; it can be concluded that the stiffness of the material increased with the addition CNF % and shearing.

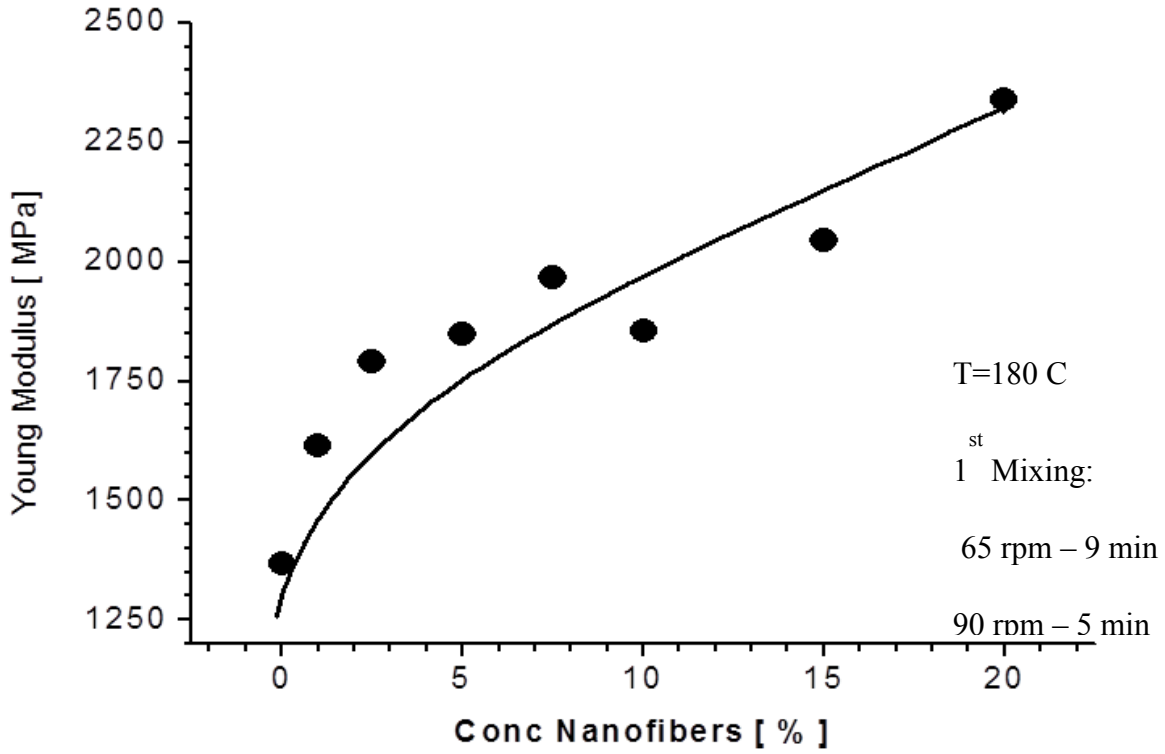

Figure 17. Young Modulus vs. CNF %

4.2 Differential Scanning Calorimetry Analysis

The results were then analyzed using the DSC to understand the thermal stability of the interface that was formed. Isothermal DSC was used to measure the heat released during the crystallization of a sample which is proportional to the mass of the crystallized material at a given temperature. It technically measures the first derivative of the Avrami equation with respect to time. It is based on rapidly cooling of the sample from the melt to crystallization temperature and then measuring the heat evolved while the sample is held isothermal. In Figure 18, the crystallization rate is shown for pure polypropylene without the addition of CNF. The time for the crystallization occurs within a time span of 45 minutes.

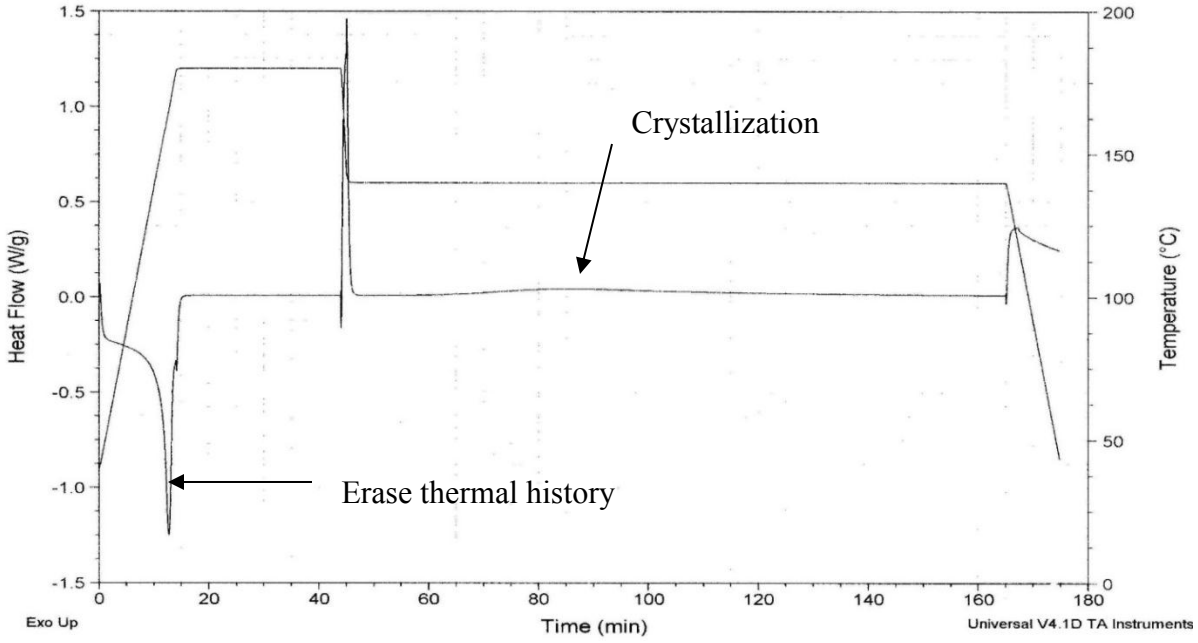

Figure 18: Heat Flow, Temperature vs. Time for Pure PP

Figure 19 shows the IPP with the addition of 2.5 % of CNF. A faster crystallization rate has occurred in comparison with the pure polymer. The time span was reduced to approximately 30 minutes.

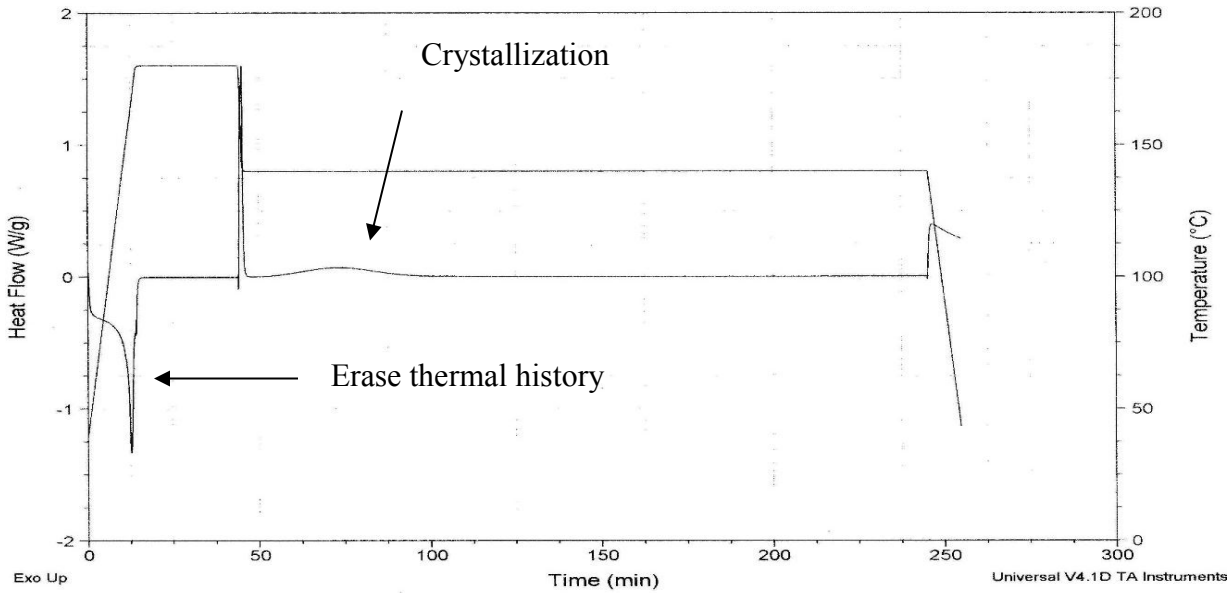

Figure 19: Heat Flow, Temperature vs. Time for 2.5% CNF reinforcement

In Figure 20 it is showed that the IPP with the addition of 10% CNF requires less time for crystallization and the peak is increasing. The surface area under the curve should be the same for all samples.

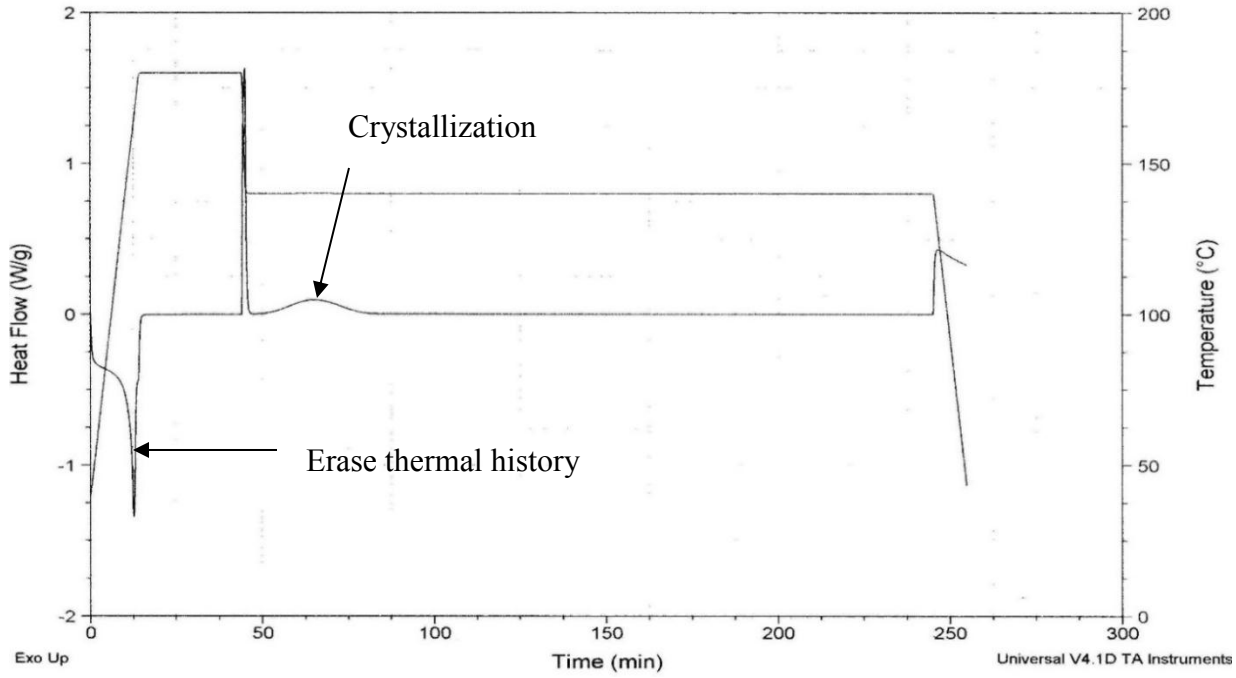

Figure 20: Heat Flow, Temperature vs. Time for 10% CNF reinforcement

The Avrami Equation was used to describe the kinetics of crystallization. The time dependence of the crystallization process at a given temperature between the glass and the melting temperature of the polymer can be described as:

$$C=c_o(1\text{-}\exp\text{-}Kt^n)$$

It describes the time dependence of the crystallization process at a given temperature between the glass and the melting temperature of the polymer. The c_o is the pre-exponential factor (initial concentration of crystallization sites), K is the reaction rate for the crystallization process, t is the crystallization time, and n is the dimensionality of the crystallization process (typically ranging between 0.5 and 4. In the initial theory was supposed to be 1, 2, or 3). [38] The experimental data received from the DSC results would be compared to this equation.

Figure 21 - 25 shows the isothermal DSC at 135 °C, 137.5 °C, 140 °C, and 142.5 °C.

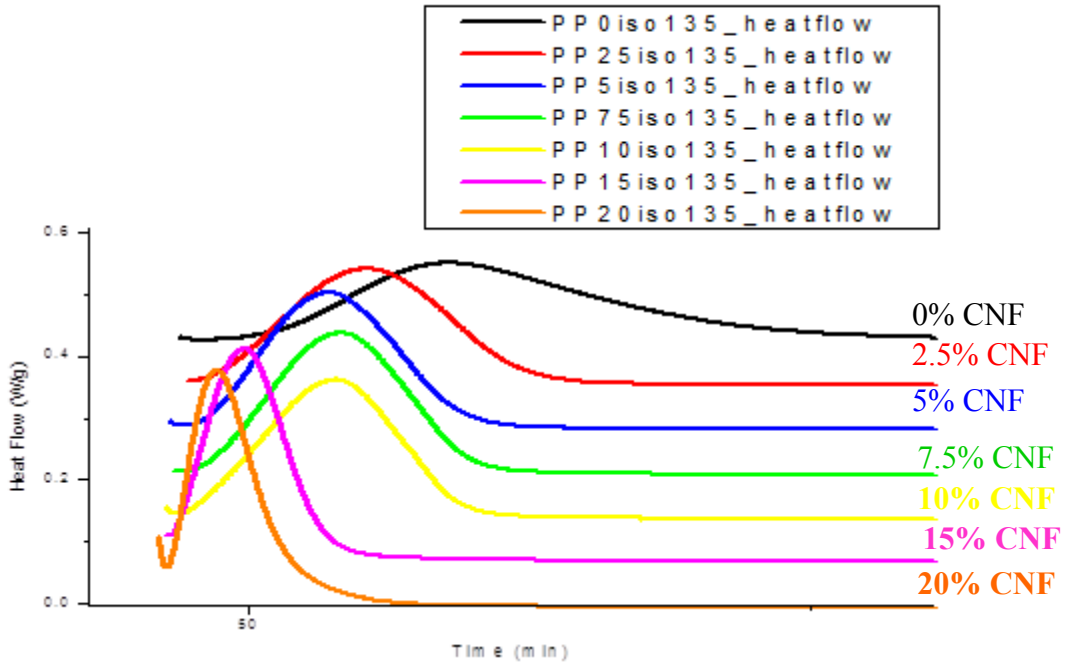

Figure 21: Heat Flow vs. Time for Isothermal DSC at 135 °C

In Figure 21, the crystallization rate shows an increase as the increase of CNF percentage increases.

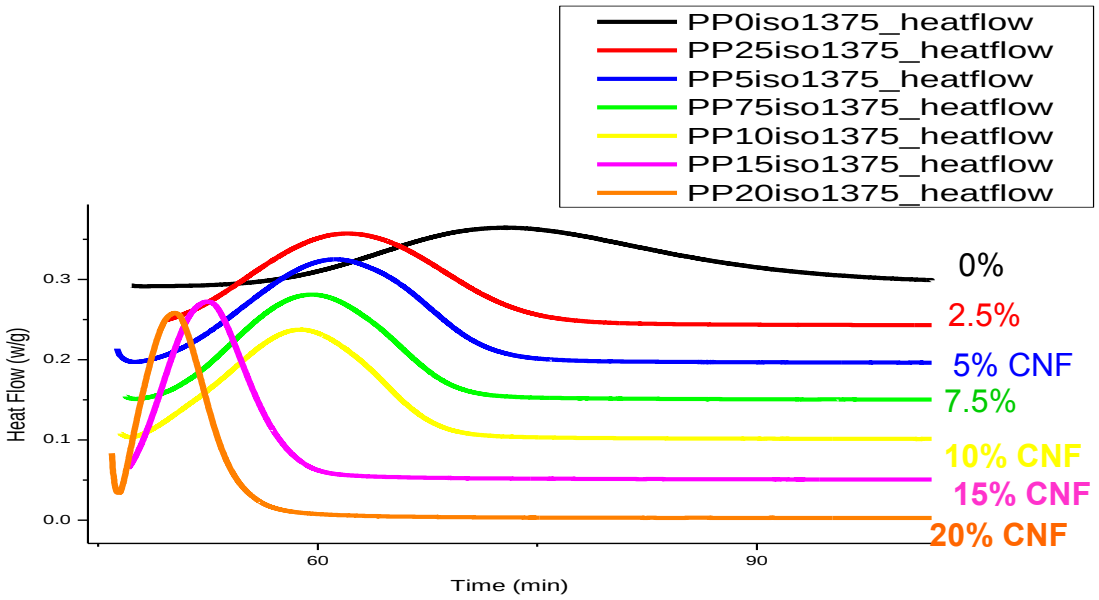

Figure 22: Heat Flow vs. Time for Isothermal DSC at 137.5 °C

The Figure 22 shows that at an isothermal temperature of 137.5 °C the crystallization rate is increasing.

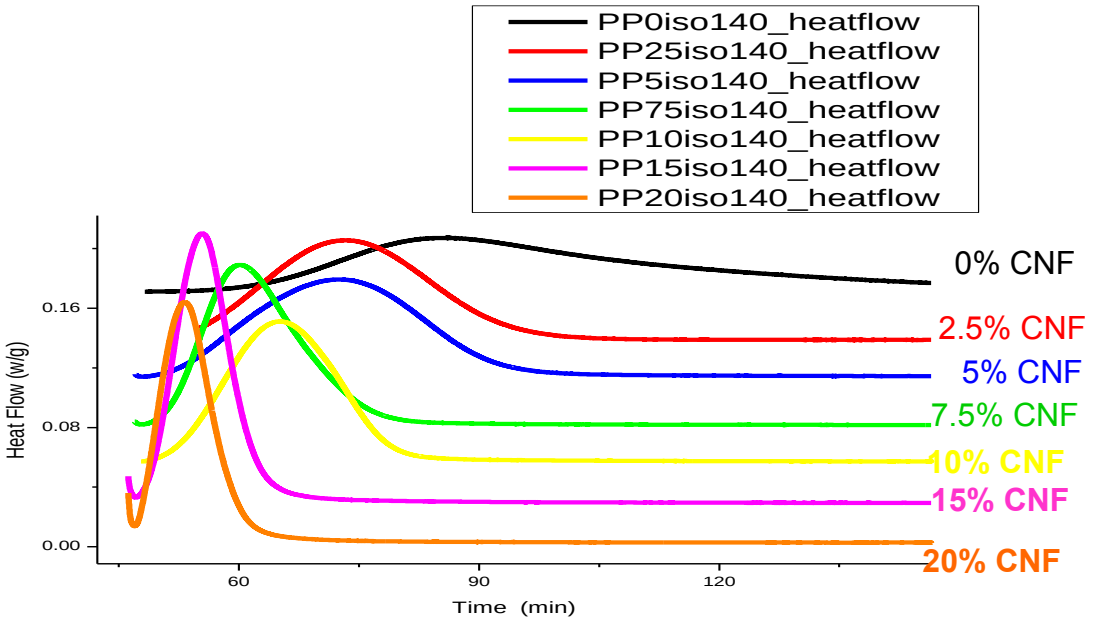

Figure 23: Heat Flow vs. Time for Isothermal DSC at 140 °C

The Figure 23, isothermal temperature at 140 °C, shows that the crystallization rate is occurring faster as compared to the rate at previous temperature of 137.5 °C.

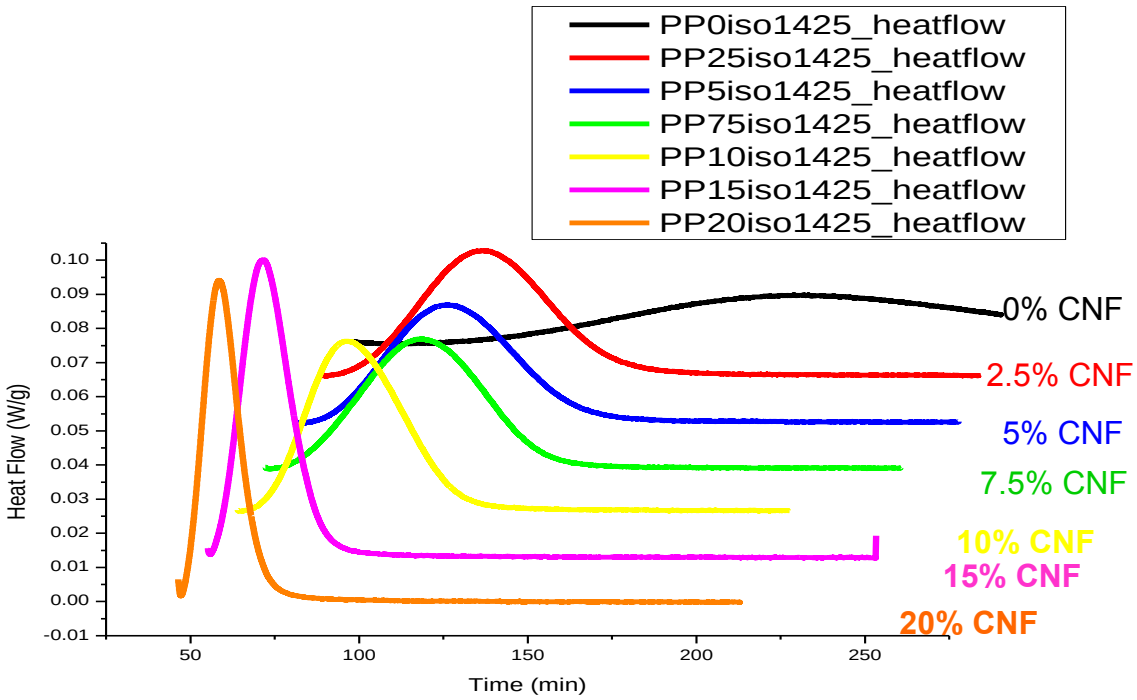

Figure 24: Heat Flow vs. Time for Isothermal DSC at 142.5 °C

At temperatures of 142.5 °C and 145 °C, represented in Figure 24 and 25, the crystallization rate has increased with temperature and addition of CNF.

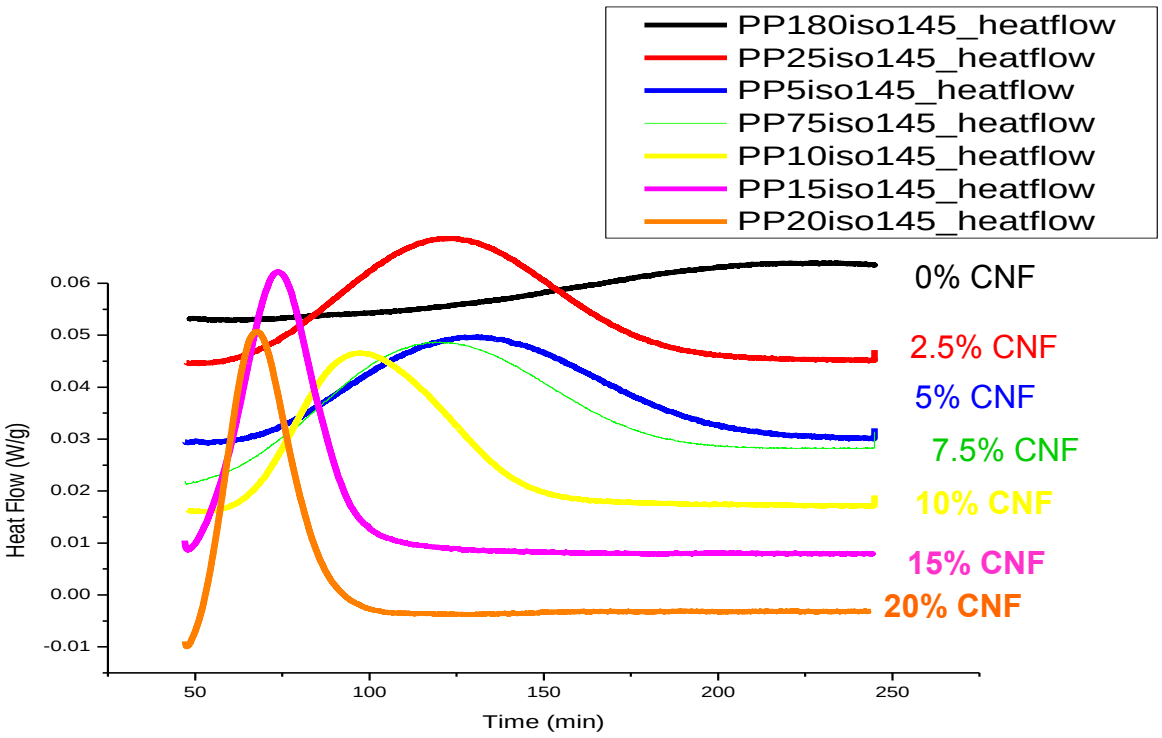

Figure 25: Heat Flow vs. Time for Isothermal DSC at 145 °C

In a lower temperature, with the addition of CNF percentage, the sample was not crystallizing fast enough which meant it was not a fully crystallized material. This means when it is exposed to a higher temperature the composite could distort. In comparison, at a higher temperature, the crystallization could also not be completely formed.

Using the information from the graphs above, the CNF percentage was then graphed according to the different isothermal temperatures. Figure 26 shows the crystallization rate of pure polypropylene at different isothermal temperatures increasing with temperature increase.

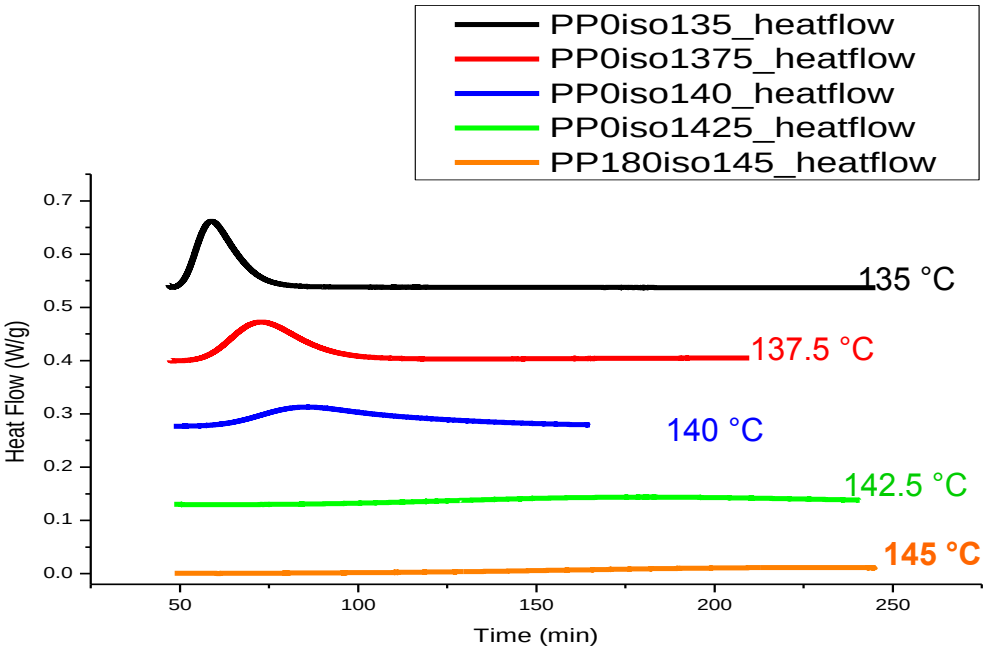

Figure 26: Heat Flow vs. Time for Pure PP at Different Isothermal Temperatures.

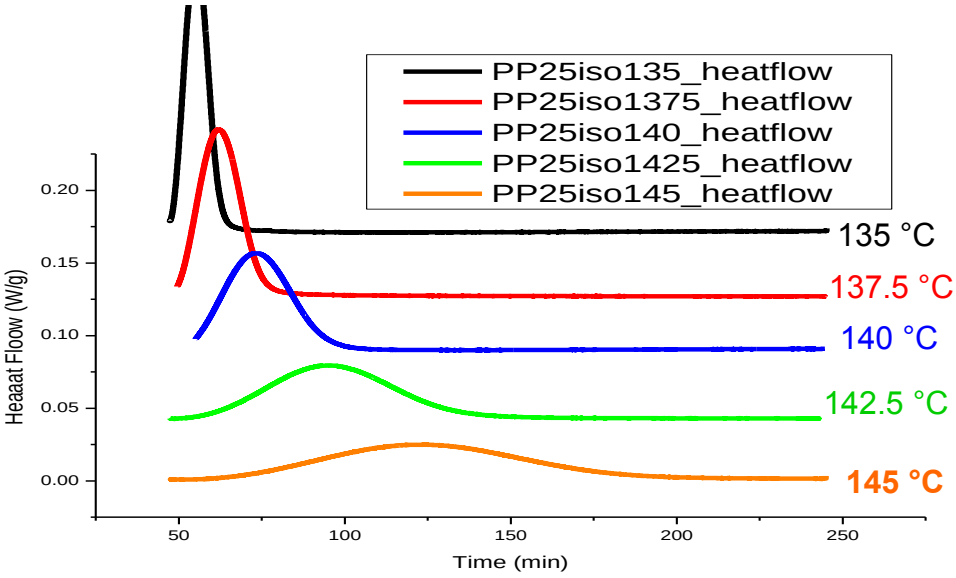

Figure 27: Heat Flow vs. Time for CNF 2.5% at Different Isothermal Temperatures

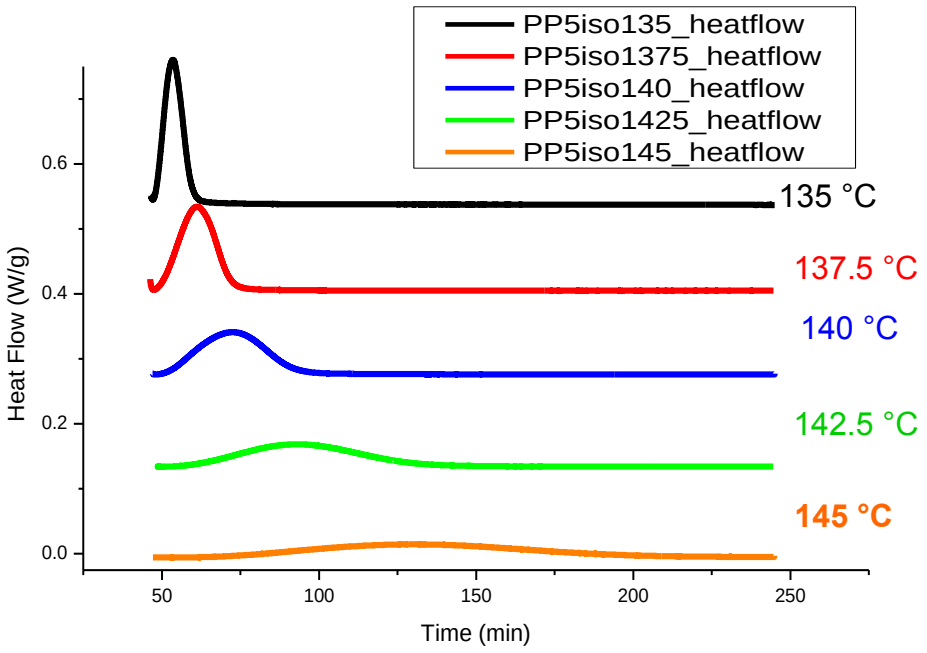

Figure 28: Heat Flow vs. Time for CNF 5% at Different Isothermal Temperatures

Figure 27 and 28 shows that the 2.5 and 5 % CNF addition has a better crystallization rate in comparison with the other CNF percentages.

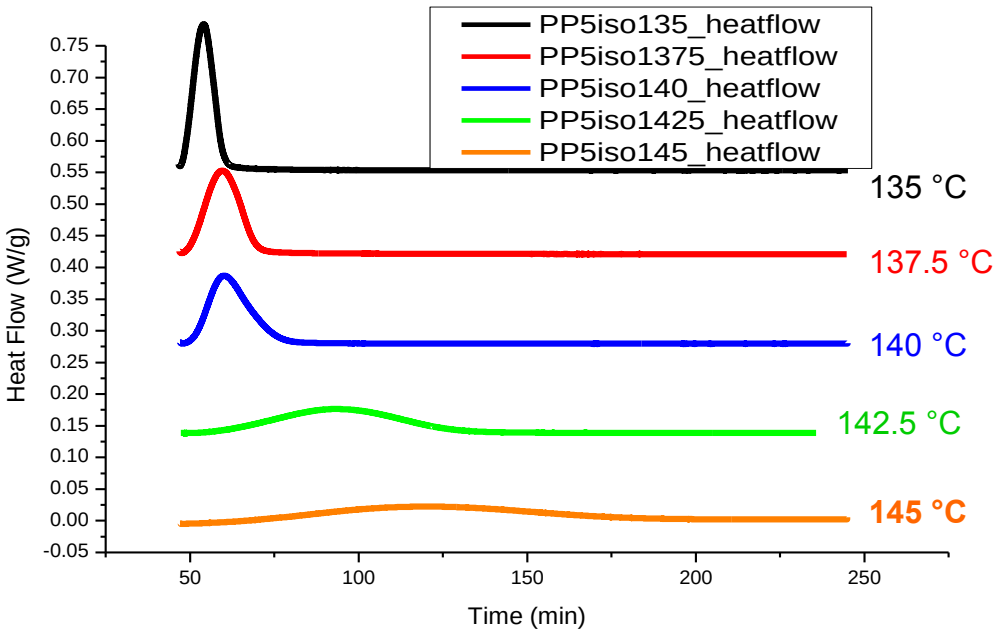

Figure 29: Heat Flow vs. Time for CNF 7.5% at Different Isothermal Temperatures

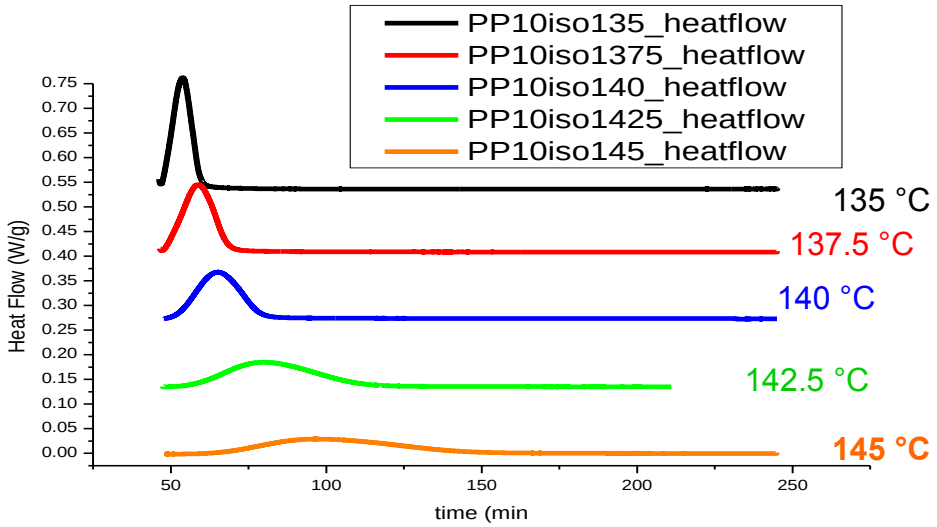

Figure 30: Heat Flow vs. Time for CNF 10% at Different Isothermal Temperatures

In Figure 29 and 30, the crystallization appears to be occurring with the same rate even though there is an increase of CNF.

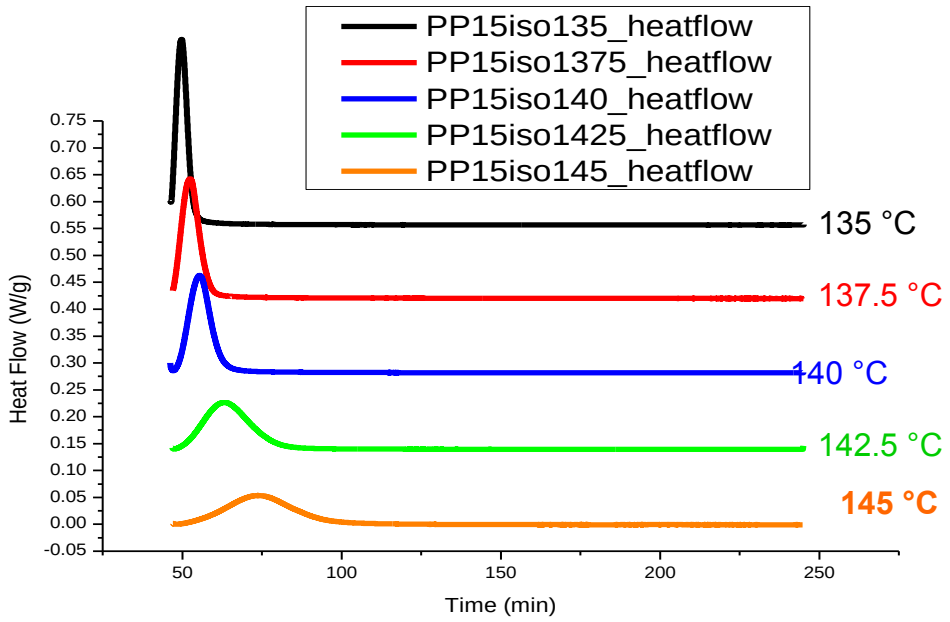

Figure 31: Heat Flow vs. Time for CNF 15% at Different Isothermal Temperatures

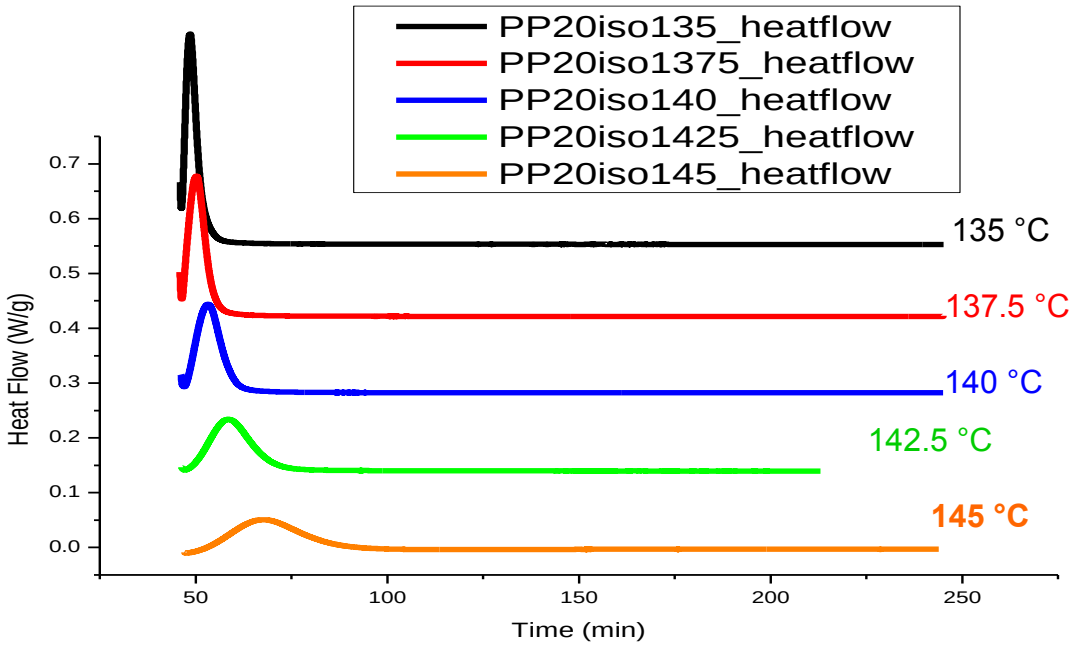

Figure 32: Heat Flow vs. Time for CNF 20% at Different Isothermal Temperatures

Figures 31 and 32 shows the crystallization rate has increased but has no significant difference with the addition of CNF or temperature.

After the samples were analyzed using the DSC, the modified Avrami equation was used. [38] The samples were then fitted with the experimental data by a modified Avrami equation:

$$C=c_o(1-\exp-(a(t-t_o))^{n)} \text{ (Modified AVRAMI)}$$

- $K= a^n$
- t_o= fitting parameter

FITTING EQUATION:

- term=(A*(x-M))^N;
- y=(C*term/(x-M))*(exp(-term))+B;
- With: M=t_o, N=n, C=c_o, x=t, B, C fitting parameters

In Figures 33 - 41, the experimental data is shown in black and the best fit line is shown in red.

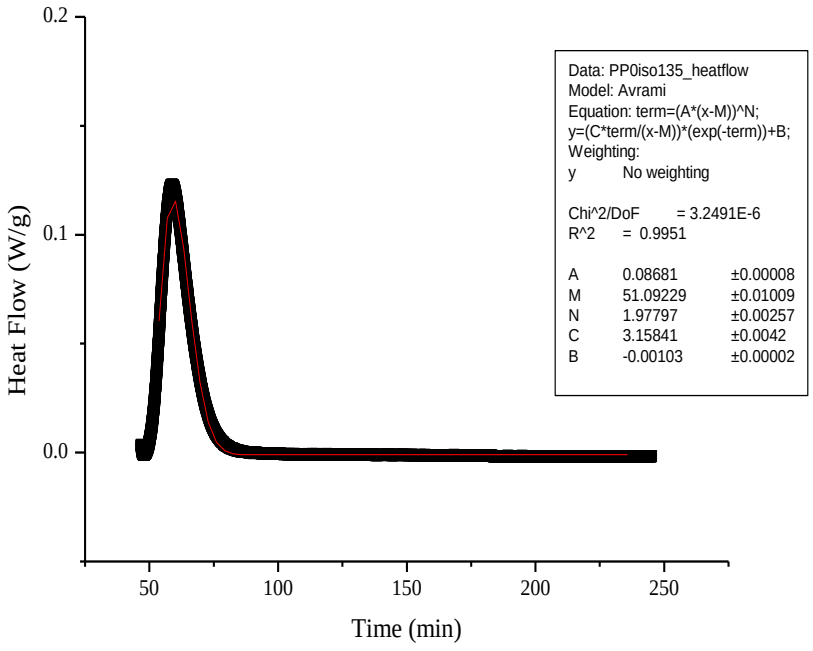

Figure 33: Heat Flow vs. Time for PP Pristine 135 ^oC

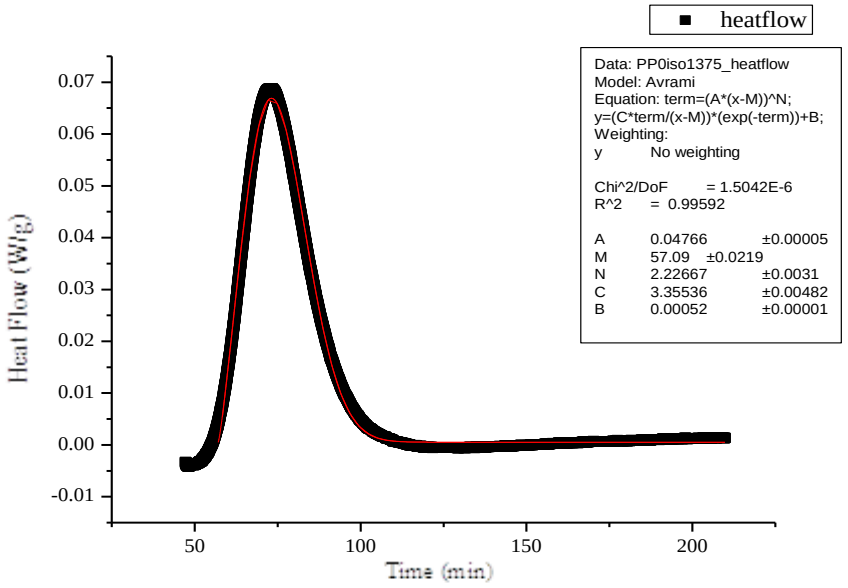

Figure 34: Heat Flow vs. Time for PP Pristine 137.5 ^{o}C

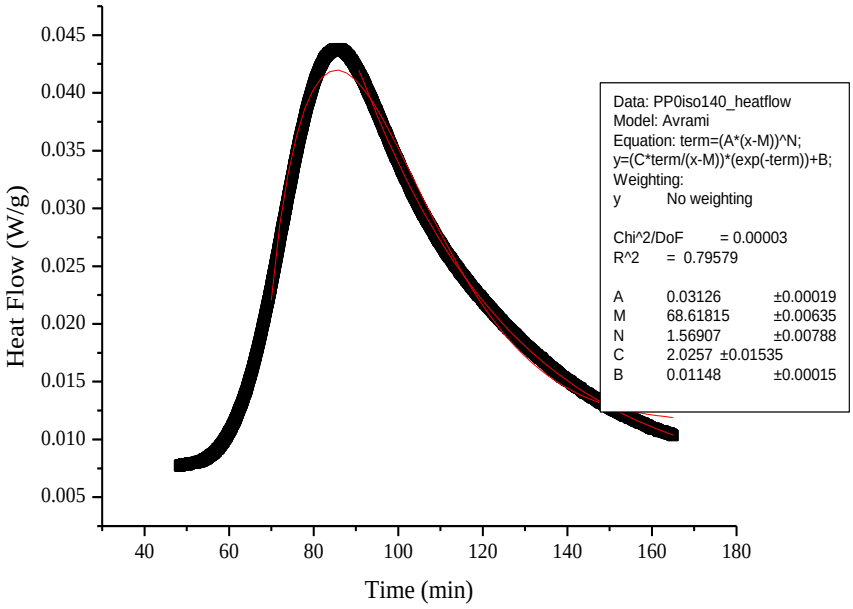

Figure 35: Heat Flow vs. Time for PP Pristine 140 ^{o}C

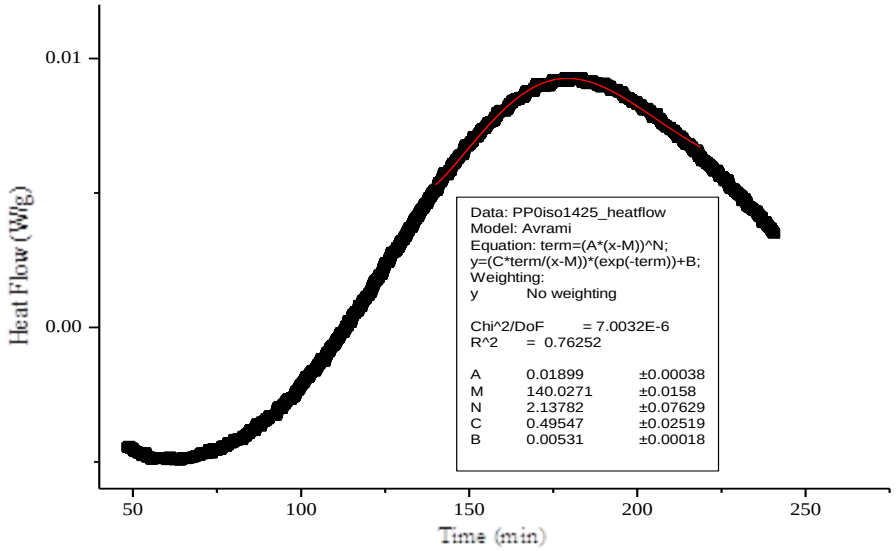

Figure 36: Heat Flow vs. Time for PP Pristine 142.5 ^{o}C

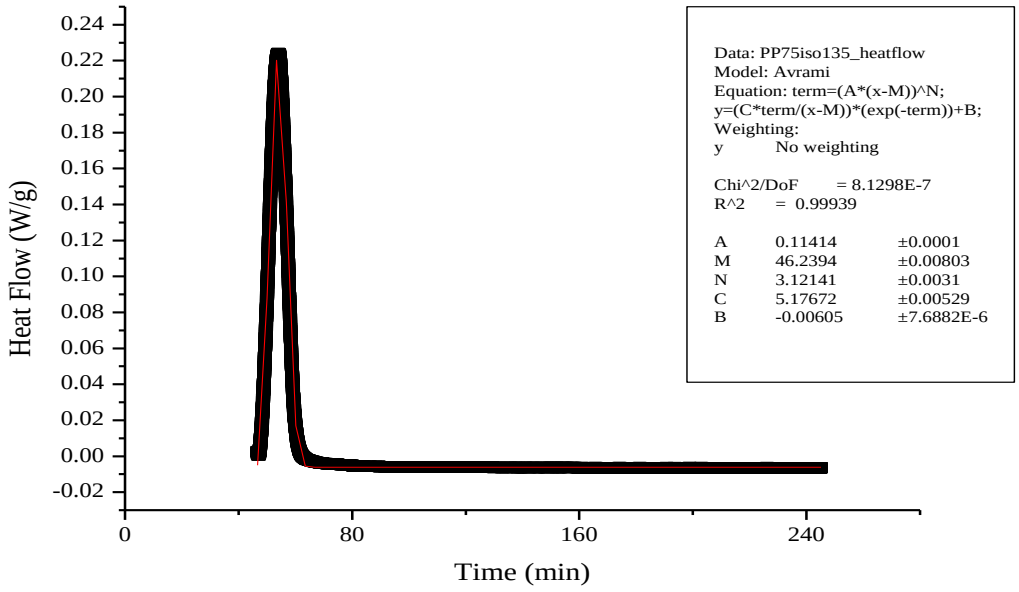

Figure 37: Heat Flow vs. Time for PP 7.5% CNF at 135 ^{o}C

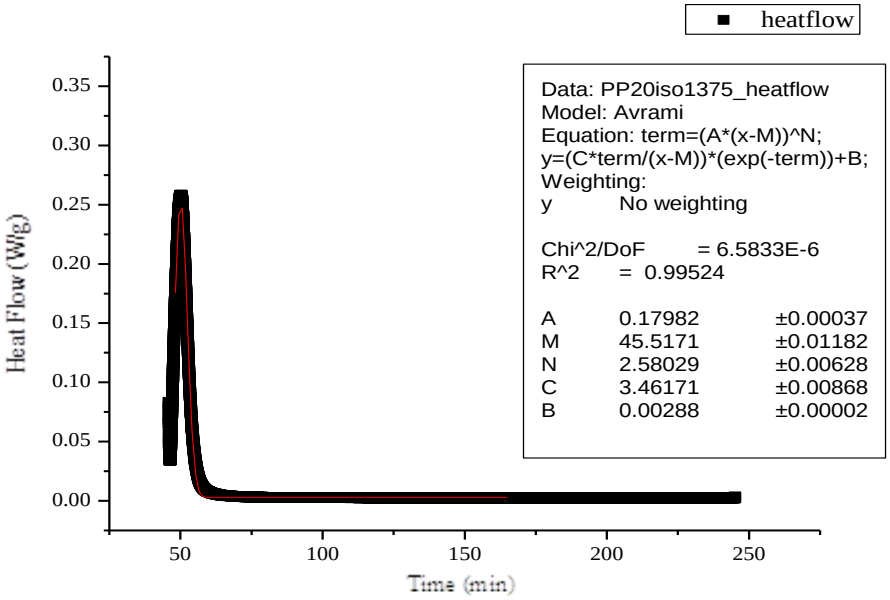

Figure 38: Heat Flow vs. Time for PP 7.5% CNF at 137.5 °C

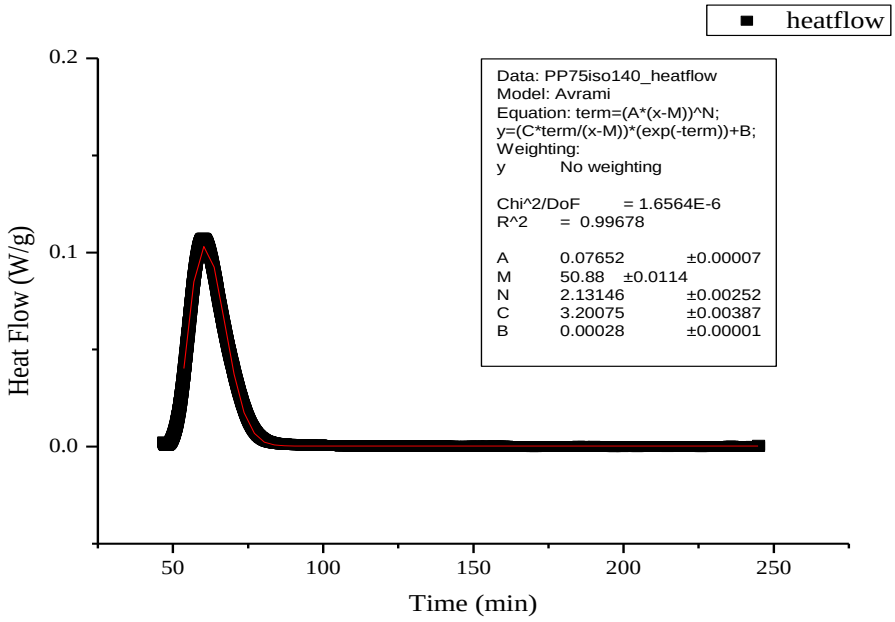

Figure 39: Heat Flow vs. Time for PP 7.5% CNF at 140 °C

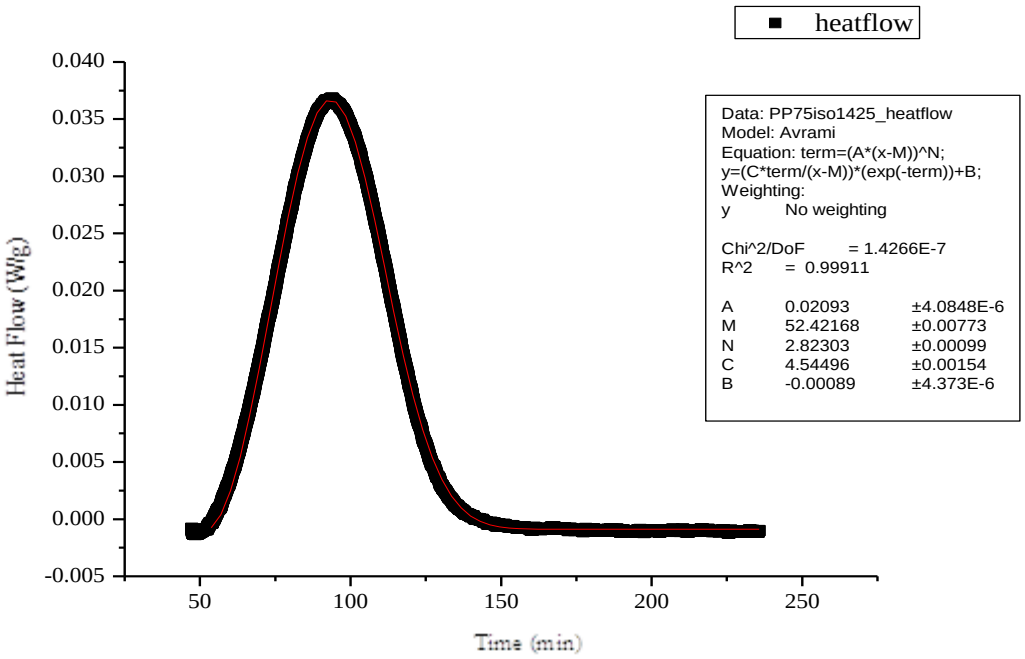

Figure 40: Heat Flow vs. Time for PP 7.5% CNF at 142.5 ^{o}C

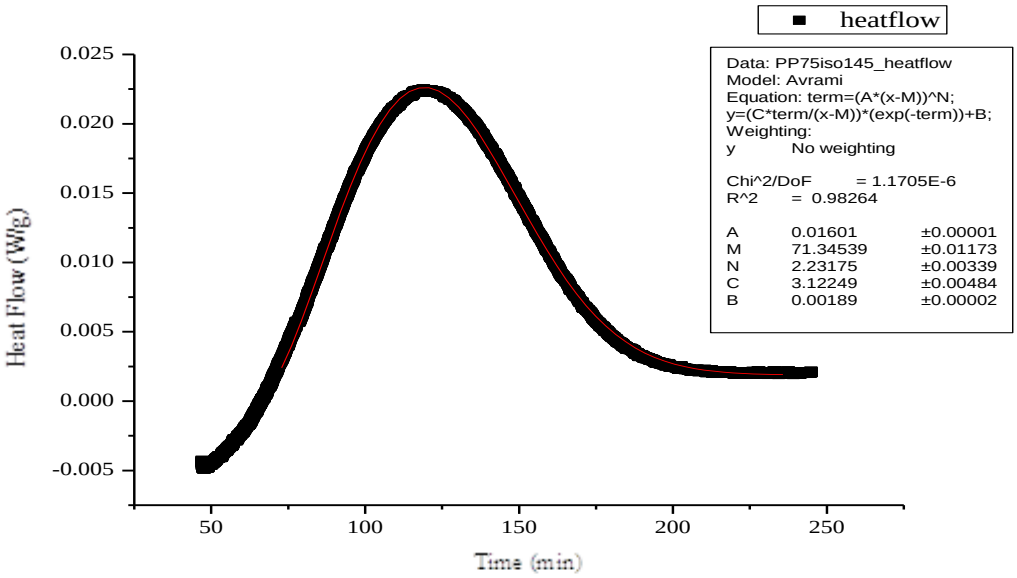

Figure 41: Heat Flow vs. Time for PP 7.5% CNF at 145 ^{o}C

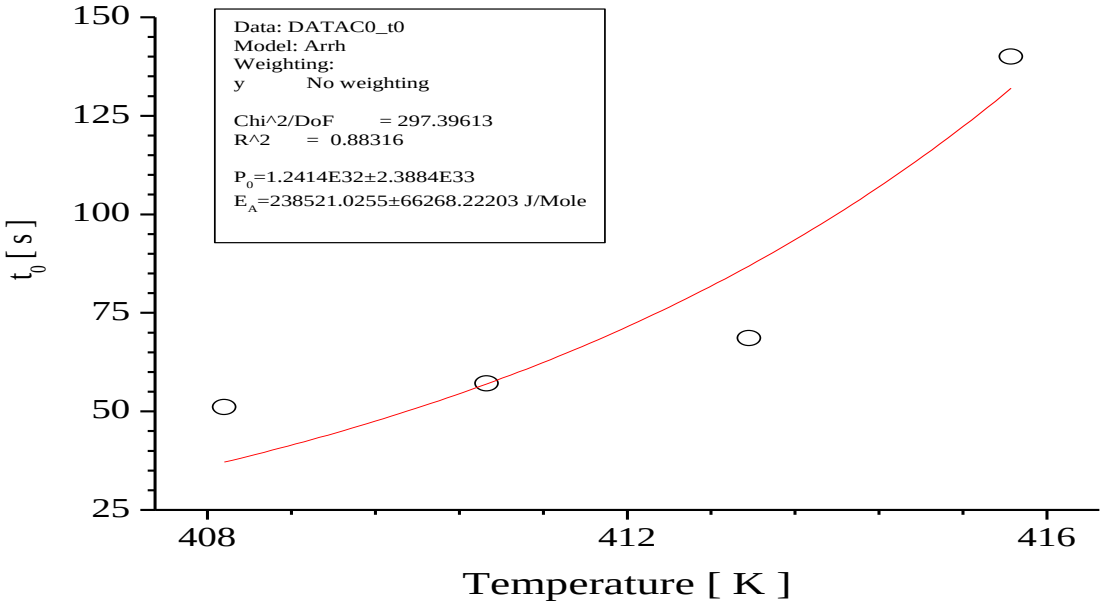

Figure 42: Pristine PP - Induction vs. Temperature

The information was then used to obtain the induction time, the reaction rate and the Avrami reaction rate dependence on temperature.

In Figure 42, t_0 has an Arrhenius – like dependence on temperature where t_o is the induction time.

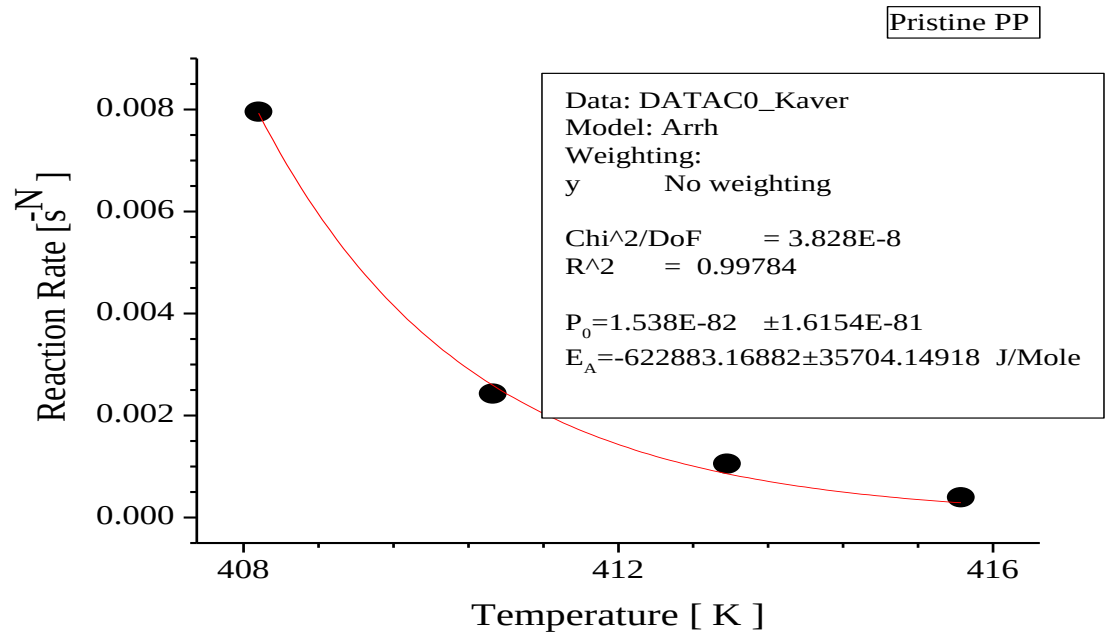

Figure 43: Pristine PP - Reaction rate vs. Temperature

Figure 43 shows the Avrami reaction rate, K, has an Arrhenius – like temperature dependence.

The reaction rate decreases with the increase of temperature.

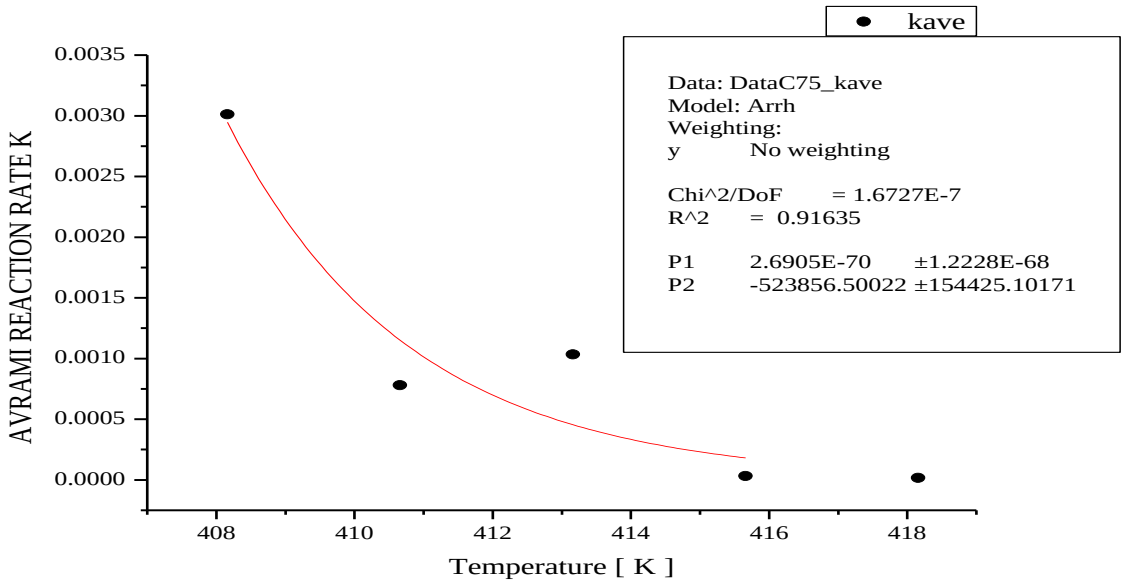

Figure 44: IPP w/ CNF 7.5 %Avrami Reaction Rate vs. Temperature

Figure 44 shows the Avrami crystallization rate constant, K, it also has an Arrhenius-like temperature dependence.

4.3 Thermogravimetric Analysis

The temperature dependence of the sample mass of the composites (ranging from 0% to 20% wt. CNF) are shown in the Figure 45. The thermal degradation of IPP shifts towards higher temperature as the increase of CNF percentage. The heat is the vibration of the molecule and as the temperature increases, the more molecules vibrate trying to break apart. In this case, the nanofibers are acting as pinned down for the molecular vibration.

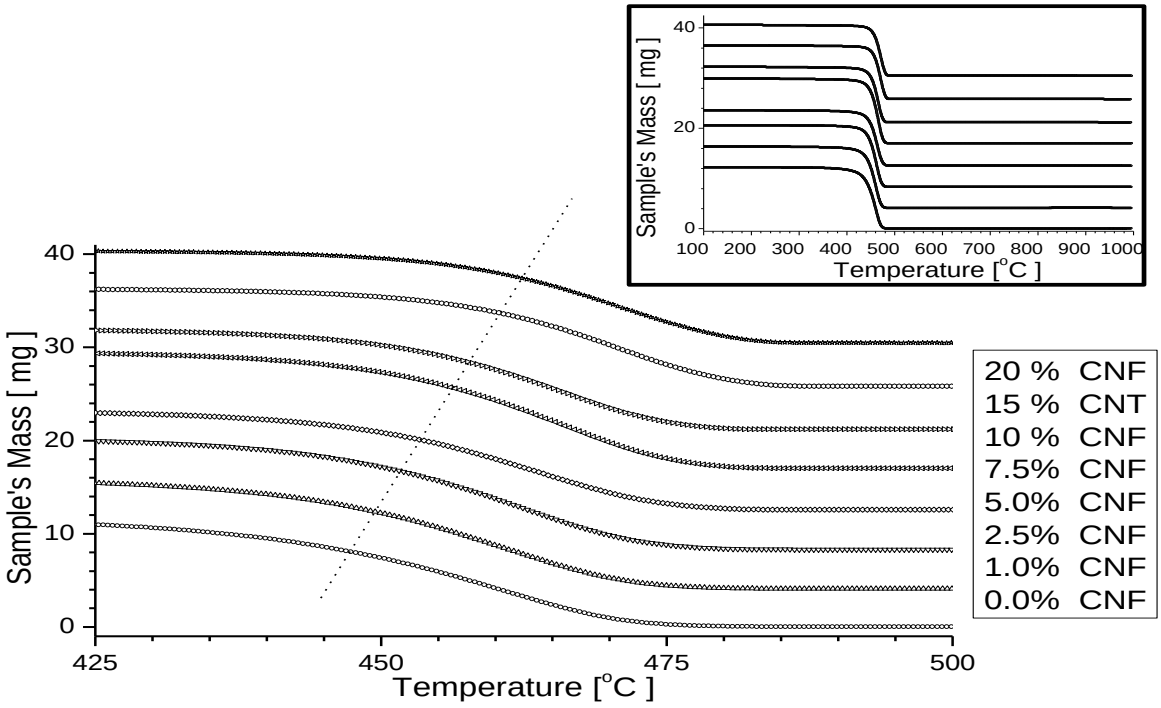

Figure 45: Sample mass vs. Temp at different CNF %

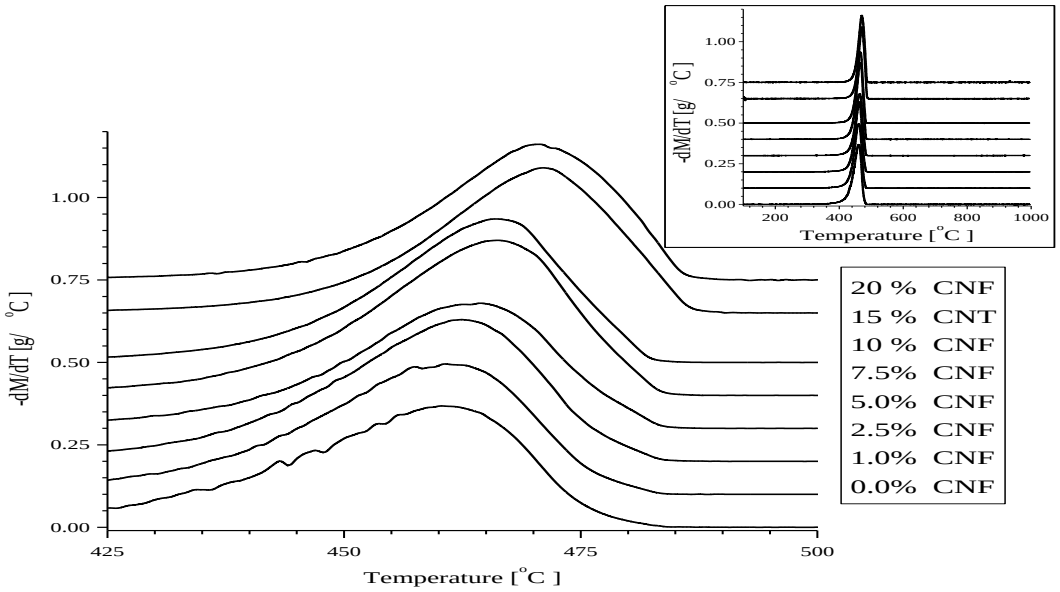

Figure 46: First derivative of the mass loss vs. Temp at different CNF %

In the Figure 46, the first derivative of the mass loss versus the degradation temperature is shown. The derivative of the residual mass as a function of temperature has a single maximum, is asymmetric, and shifts towards higher temperatures with the addition of VGCNFs.

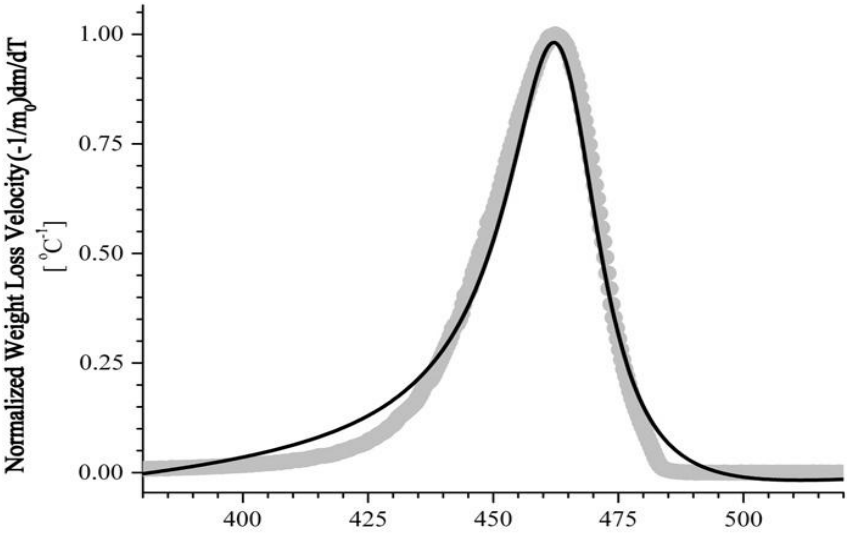

Figure 47: Normalized Weight Loss Velocity vs. Temperature

The first derivative of the sample's mass relative to the sample's temperature as a function of temperature was represented in Figure 47. The temperature at which the mass loss rate is maximum is estimated (the inflection temperature).

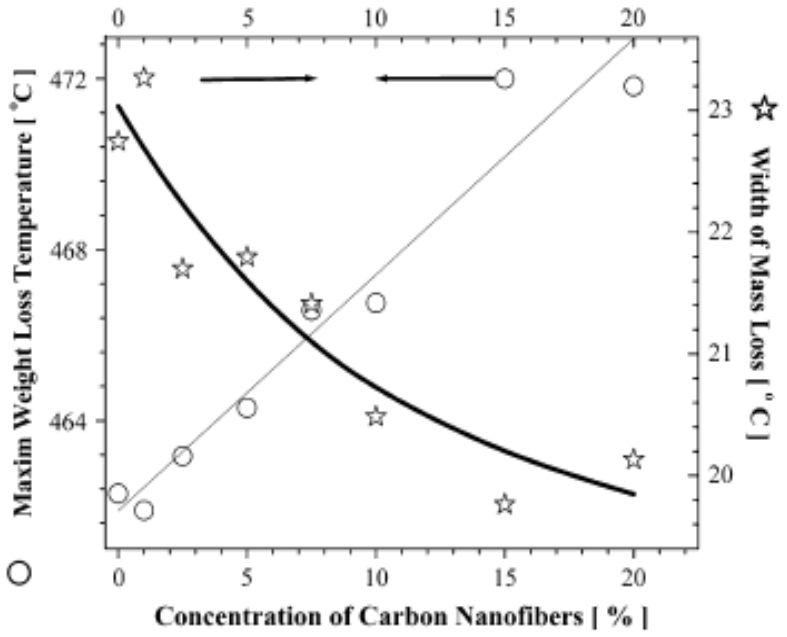

Figure 48: Maxim Weight Loss Temperature, Width of Mass Loss vs. Conc. of CNF %

In the Figure 48, left axis, open circles show the effect of loading with VGCNFs on the temperature at which the thermal degradation is maximum. In the right axis, the stars show the effect of loading with VGCNFs on the width of the degradation process.

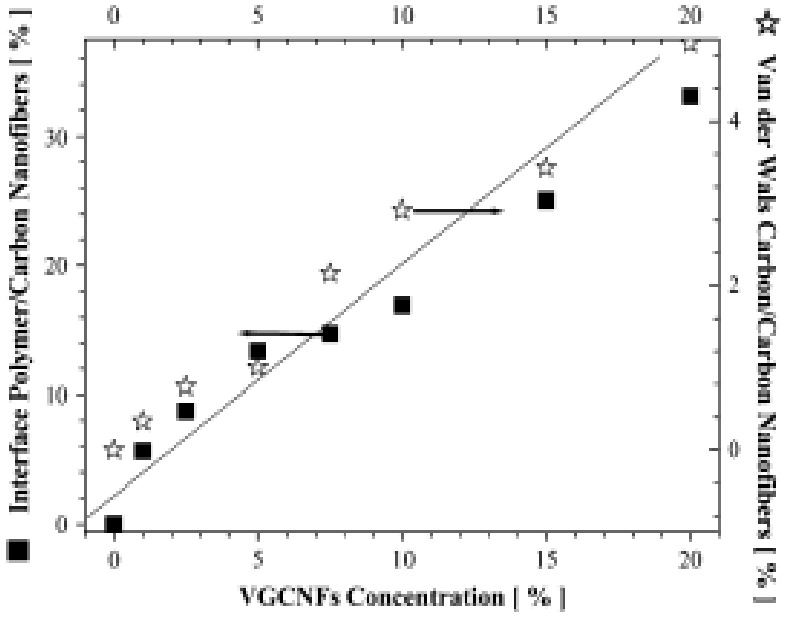

Figure 49: Interface Polymer/CNF %, Van der Waals Carbon/CNF % vs. VGCNF %

In Figure 49, the left axis, the filled squares show the dependence of the fraction of polymer chains captured in the elastic layer of the interface on the polymer loading with VGCNFs. The right axis, stars are showing the dependence of the fraction of polymer chains captured in the hard layer of the interface on the polymer loaded with VGCNFs.

4.4 Transmission Electron Microscopy Analysis

The TEM image, Figure 50, was used to check for the dispersion of the nanofiller within the polymeric matrix. The degree of dispersion resulted in a very large surface area and explained the effect of the interface on the macroscopic thermal stability.

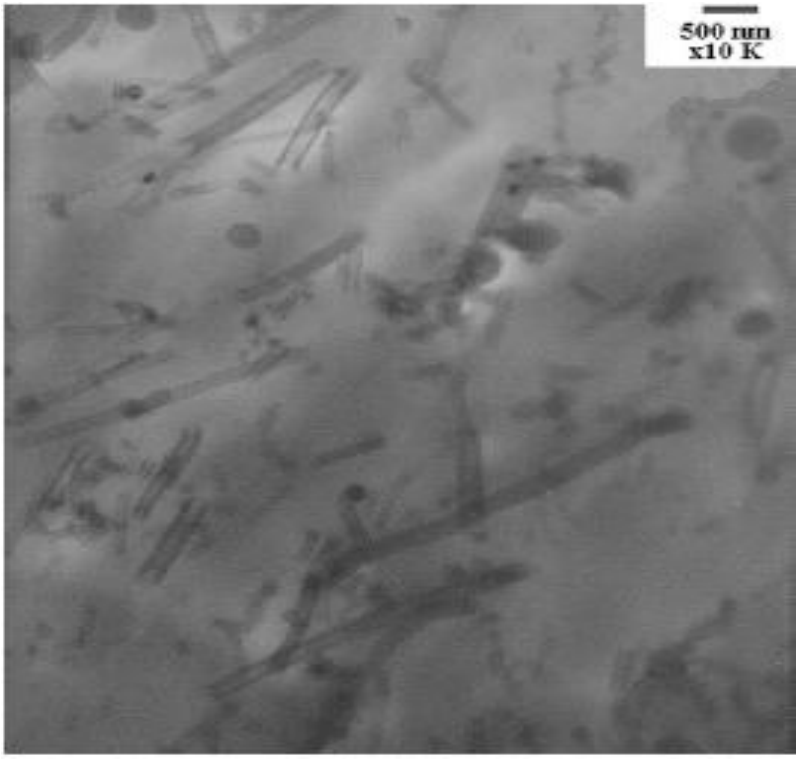

Figure 50: TEM micrograph of IPP-VGCNF composites loaded with 20% wt. VGCNFs

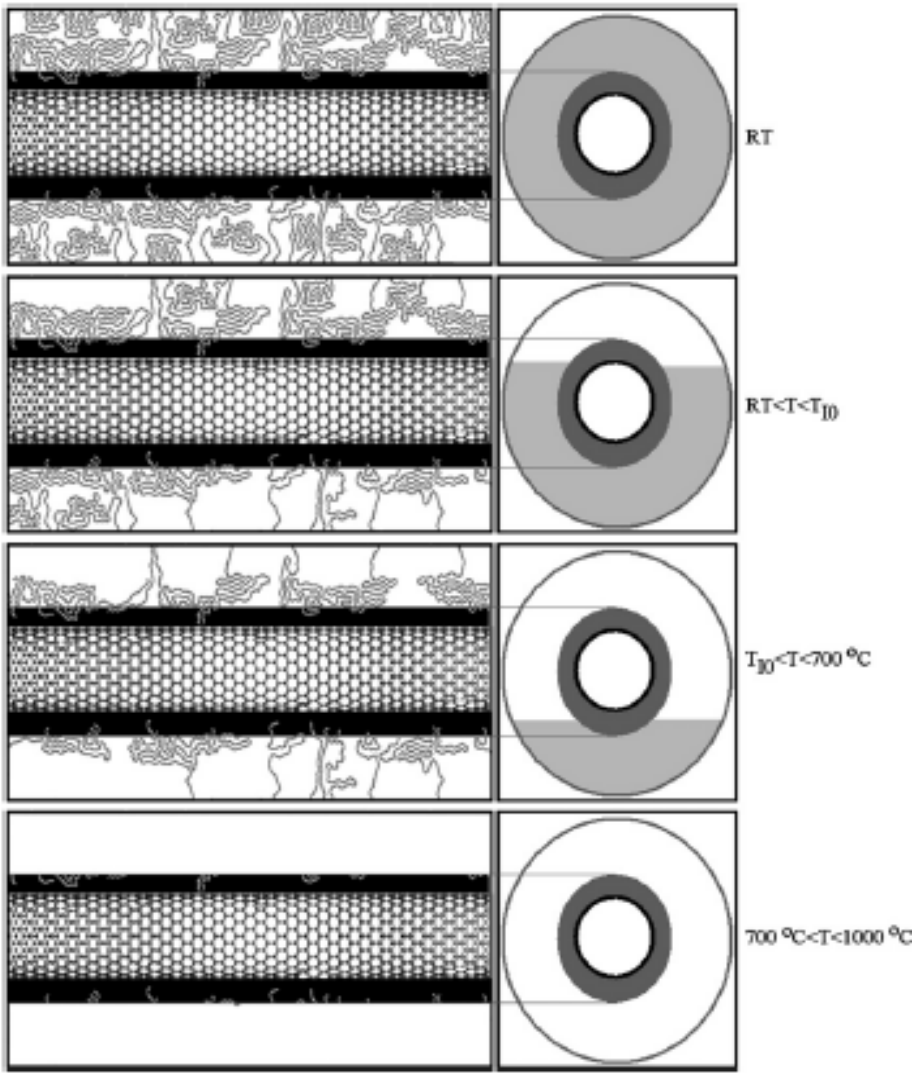

Figure 51: Model of Adhesion of PP to VGCNFs

An explanation of the interface of the IPP-CNF interface can be seen in the Figure 51, the model of adhesion of PP to VGCNFs. The first panel shows the morphology at room temperature. The second panel is the morphology at a temperature lower than the temperature at which the mass loss is maximum (T_{I0}). Due to the molecular motion, some of the macromolecular chains that are interacting with the VGCNFs have been removed. The third panel shows the immediately above temperature at which the maximum mass loss is reached. In this panel, the macromolecular

chains interaction with VGCNFS shows a decrease in density. The last panel shows the VGCNFs above 700 ºC, at this temperature the polymer is fully vaporized and only the molecules trapped by the Van der Waals interactions are left on the VGCNFs.

CHAPTER V

SUMMARY AND CONCLUSION

An observed enhancement of the thermal stability of IPP by the loading with VGCNFs is a direct proof for the existence of an IPP-VGCNFs interface. Mathematical modeling provided quantitative estimations on the inflection temperature shift. It suggested a better homogenization of the temperature distribution within the nanocomposite. The experimental data showed that there was two-layer structure formed in the composite. An external layer showed a thickness comparable to the radius of gyration of the polymer and contributes to the enhanced thermal stability of the composite. The IPP-VGCNFs showed thickness has been estimated to be of the order of 10^2 nm. The TGA analysis showed a new inner layer with a thickness of the order of 10 nm. The layer is tentatively assigned to those molecules belonging to VGCNFs that are located around VGCNFs at distances smaller or equal to 10 nm. The dispersion of VGCNFs within the IPP, as shown by the TEM micrograph, supports the proposed interpretation. Future research will focus on a better understanding of the fabrication methodologies, processing parameters, morphology characterization, and fundamental physics in order to obtain better interface, dispersion, and distribution.

This work has been peer reviewed and published as Magdalena Chipara, Karen Lozano, Anna Hernandez, Mircea Chipara, TGA analysis of polypropylene–carbon nanofibers composites, Polymer Degradation and Stability. It was the top 25 viewed article in the year of 2008. The article can be seen in Appendix A.

REFERENCES

[1] Osswald, T.S. and G. Menges, “Materials Science of Polymers for Engineers”, Hanser Verlag, Munich, 1995.

[2] Edgar Munoz, Alan B. Dalton, Steve Collins, Mikhail Kozlov, Joselito Razal, Jonathan N. Coleman, Bog G. Kim, Von Howard Ebron, Miles Selvidge, John P. Ferraris, Ray H. Baughman. "Multifunctional carbon nanotube composite fibers." Advanced Engineering Materials 2004 6(10), 801-804.

[3] H. Daniel Wagner and Richard A. Vaia, Nanocomposites: issues at the interface, Materials Today, Volume 7, Issue 11, November 2004, Pages 38-42.

[4] Milo Shaffer and Ian A. Kinloch, Prospects for nanotubes and nanofiber composites, Composites Science and Technology, Volume 64, Issue 15, November 2004, Pages 2281-2282.

[5] E. Hammel, X. Tang, M. Trampert, T. Schmitt, K. Mauthner, A. Eduer, and P. Potschke. Carbon nanofibers for composite applications, Carbon, Volume 42, February 2004, Pages 1153-1158.

[6] Hui Zhang and Zhong Zhang. Impact behavior of polypropylene filled with multi-walled carbon nanotubes, European Polymer Journal, Articles in Press.

[7] M.A. Lopez Manchado, Lvalentini, J. Biagiotti, and J.M. Kenny. Thermal and mechanical properties of single-walled carbon nanotubes – polypropylene

composites prepared by melt processing, Carbon, Volume 43, March 2005, Pages 1499-1505.

[8] Jijun Zeng, Bethany Saltysiak, W. S. Johnson, David A. Schiraldi, and Satish Kumar. Processing and properties of poly(methyl methacrylate)/ carbon nanofiber composites, Composite Part B: engineering, Volume 35, January 2003, Pages 245 – 249.

[9] Erik T. Thostenson and Tsu-Wei Chou. Aligned multi-walled carbon nanotubes-reinforced composites: processing and mechanical characterization, Journal of Physics D; Applied Physics, Volume 35, August 2002, Pages L77- L80.

[10] M.L. Shofner, F.J. Rodriguez-Macias, R. Vaidyanathan, and E.V. Barrera. Single wall nanotube and vapor grown carbon fiber reinforced polymers processed by extrusion freeform fabrication, Composites Part A: applied science and manufacturing, Volume 34, July 2003, Pages 1207 – 1217.

[11] Carole A. Cooper, Diana Ravich, David Lips, Joerg Mayer, and H. Daniel Wagner. Composites Science and Technology, Volume 62, March 13, 2002, Pages 1105 – 1112.

[12] Han Gi Chae, Marilyn L. Minus, and Satish Kumar. Oriented and exfoliated single wall carbon nanotubes in polyacrylonitrile, Polymer, Volume 47, April 3, 2006, Pages 3494-3504.

[13] D.C. Bassett, Polymer Morphology: A Guide to Macromolecular Self-Organization, Macromol. Symp., 2004, 214, Pages 5-15.

[14] D.C. Bassett, Polymer spherulites: a modern assessment, J Macromol Sci, Phys B 42 (2003), pp. 227–256.

[15] Yu Long, Robert A. Shanks and Zbigniew H. Stachurski, Kinetics of polymer crystallization, Progress in Polymer Science, Volume 20, Issue 4, 1995, Pages 651-701.

[16] M. I. Abo el Maaty and D.C. Bassett, New Contexts for Polymer Crystallization, Journal of Macromolecular Science Part B – Physics, Vol. B42, Nos. 3 & 4, 2003, Pages 687-695.

[17] J. Varga , Supermolecular structure of isotactic polypropylene. J. Mater. Sci. 27 (1992), pp. 2557–2579

[18] B. Lotz, J. C. Wittmann and A. J. Lovinger, Structure and morphology of poly(propylenes): a molecular analysis, Polymer, Volume 37, Issue 22, Symposium commemorating the 35th anniversary of Polymer, October 1996, Pages 4979-4992.

[19] Marigo, Antonio, Marega Carla, Causin, Valerio, and Ferraari, Paolo, Influence of Thermal Treatments, Molecular Weight, and Molecular Distribution on the crystallization of β-Isotactic Polypropylene, Journal of Applied Polymer Science, Volume 91, June 2003, Pages 1008- 1012.

[20] Marco, C., Gomez, M.A., Ellis, G. and Arribas, J.M., Activity of a β-Nucleating Agent for Isotactic Polypropylene and Its Influence on Polymorphic Transitions, Journal of Applied Polymer Science, Volume 86, October 29, 2001, Pages 531 – 539.

[21] Lotz, B., α and β phases of isotactic polypropylene: a case of growth kinetics 'phase reentrency' in polymer crystallization, Polymer, Volume 39 No. 19, September 19, 1997, Pages 4561-4567.

[22] Dorset, D. L., McCourt, M.P., Kopp, S., Schumacher, M., Okihara, T., and Lotz, B., Isotactic polypropylene, β-phase: a study in frustration, Polymer, Volume 39 No. 25, September 26, 1997, Pages 6331 – 6337.

[23] S.V. Meille, D.R. Ferro, S. Brückner, A.J. Lovinger, F.J. Padden. Structure of β-isotactic polypropylene: a long-standing structural puzzle. Macromolecules, 27 (1994), pp. 2615–2622.

[24] Menyhárd, A.; Varga, J.; Molnár, G., Comparison of different -nucleators for isotactic polypropylene, characterization by DSC and temperature-modulated DSC (TMDSC) measurements, Journal of Thermal Analysis and Calorimetry, Volume 83, Number 3, March 2006 , pp. 625-630(6).

[25] K. Lozano, A. Zheng, B. Mayeaux, N. Espinoza, L. Yoell, V. Provenzano, R. Shull, B. Files, J. Bonilla Rios, and E.V. Bareera, Fullerenes and Nanotubes: Current Research and Future Directions, Ron Dagani, Carbon Nanotube Ropes: Moving closer to practical materials, News of the week, July 29, 1996, pp. 5-6.

[26] T. Belin and F. Epron, Characterization methods of carbon nanotubes: a review, Materials Science and Engineering B, Volume 119, February 2005, pp105-118. H. Barber, I. Kaplan-Ashiri, S. R. Cohen, R. Tenne, H.D. Wagner, Composites science and technology, Volume 65, September 2005, pp. 2380-2384.

[27] Jean Paul Salvetat-Delmotte and Angel Rubio, Mechanical properties of carbon nanotubes: a fiber digests for beginners, Carbon, Volume 40, December 12, 2001, pp. 1729-1734.

[28] Bernd Lahr and Jan Sandler, Carbon Nanotubes High –Strength Reinforcing Compounds for Composites, 2001, pp. 94-98.

[29] L. Valentini, J. Biagiotti, J. M. Kenny and S. Santucci, Morphological characterization of single-walled carbon nanotubes-PP composites, Composites Science and Technology, Volume 63, Issue 8, NANO-AND MICRO-COMPOSITE PROCEEDINGS OF SYMPOSIUM N, OF THE 2002 E-MRS SPRING MEETING JUNE 18-21, June 2003, Pages 1149-1153.

[30] Josef Z. Kovacs, Kjer Andresen, Jan Roman Pauls, Claudia Pardo Garcia, Michael Schossig, Karl Schulte and Wolfgang Bauhofer, Analyzing the quality of carbon nanotube dispersions in polymers using scanning electron microscopy, Carbon, Volume 45, Issue 6, May 2007, Pages 1279-1288.

[31] Claudio De Rosa, Finizia Auriemma, Giordano De Lucia and Luigi Resconi. From stiff plastic to elastic polypropylene: Polymorphic transformations during plastic deformation of metallocene-made isotactic polypropylene, Polymer, Volume 46, Issue 22, 24 October 2005, Pages 9461-9475.

[32] K. Lozano and E.V. Barrera, Nanofiber-reinforced thermoplastic composites. I. Thermoanalytical and mechanical analysis, *J. Appl. Polym. Sci.* **79** (2001), pp. 129–133.

[33] Ioana C. Finegan, Gary. G. Tibbetts and Ronald F. Gibson, Modeling and characterization of damping in carbon nanofiber/polypropylene composites, Composites Science and Technology, Volume 63, Issue 11, Modeling and Characterization of Nanostructured Materials, August 2003, Pages 1629-1635.

[34] L. Valentini, J. Biagiotti, J. M. Kenny and S. Santucci, Morphological characterization of single-walled carbon nanotubes-PP composites, Composites Science and Technology, Volume 63, Issue 8, NANO-AND MICRO-COMPOSITE

PROCEEDINGS OF SYMPOSIUM N, OF THE 2002 E-MRS SPRING MEETING JUNE 18-21, June 2003, Pages 1149-1153.

[35] M.A. Lopez Manchado, L. Valentini, J. Biagiotti and J.M. Kenny, Thermal and mechanical properties of single-walled carbon nanotubes-polypropylene composites prepared by melt processing, Carbon, Volume 43, Issue 7, June 2005, Pages 1499-1505.

[36] Hui Zhang and Zhong Zhang, Impact behaviour of polypropylene filled with multi-walled carbon nanotubes, European Polymer Journal, In Press, Accepted Manuscript, Available online 24 May 2007, .

[37] Mohammad M. Hasan, Yuanxin Zhou and Shaik Jeelani, Thermal and tensile properties of aligned carbon nanofiber reinforced polypropylene, Materials Letters, Volume 61, Issues 4-5, February 2007, Pages 1134-1136.

[38] Magdalena Chipara, Karen Lozano, Anna Hernandez, Mircea Chipara, TGA analysis of polypropylene–carbon nanofibers composites, Polymer Degradation and Stability, Volume 93, Issue 4, April 2008, Pages 871-87.

[39] K. Lozano, B. Files, F. Rodriguez-Macias, and E. V. Barrera; “Purification and Functionalization of Vapor Grown Carbon Fibers and Single Wall Nanotubes"; TMS Publications (1999) 333.

APPENDIX

APPENDIX A

PUBLISHED PEER REVIEWED ARTICLE

The research contained in the thesis was used in the publication of a peer reviewed article: TGA analysis of polypropylene-carbon nanofibers composites. It was the top 25 viewed article in the Journal: Polymer Degradation and Stability in 2008.

Available online at www.sciencedirect.com
ScienceDirect
Polymer Degradation and Stability 93 (2008) 871–876
Polymer Degradation and Stability
www.elsevier.com/locate/polydegstab

TGA analysis of polypropylene–carbon nanofibers composites

Magdalena Chipara [a], Karen Lozano [b], Anna Hernandez [b], Mircea Chipara [a,*]

[a] Department of Physics and Geology, University of Texas Pan American, 1201 West University Drive, Edinburg, 78541 TX, USA
[b] Department of Mechanical Engineering, University of Texas Pan American, Edinburg, 78541 TX, USA

Received 22 August 2007; received in revised form 26 December 2007; accepted 7 January 2008
Available online 12 January 2008

Abstract

TGA investigations on the thermal degradation of isotactic polypropylene–vapor grown carbon nanofibers composites in nitrogen are reported. The mass evolution as a function of temperature is a single sigmoid for both polypropylene and polypropylene loaded with carbon nanofibers. The inflection temperature of these sigmoids increases as the concentration of carbon nanofibers is increased. The width of the degradation process narrows as the concentration of carbon nanofibers is increased due to a better homogenization of the local temperature provided by the high thermal conductivity of carbon nanofibers. Thermogravimetric analysis data indicate the formation of polymer–carbon nanofiber interface. Based on TGA data, a two-layer structure is proposed for carbon nanofibers–polypropylene interface. The external layer is soft and has a thickness of about 10^2 nm that confines most polymer molecules in interaction with nanofibers. The core layer is rigid and has a thickness of the order of few nanometers.

Keywords: Polymer; Carbon nanofibers; Composite; Thermogravimetric analysis; Polymer–nanofiber interaction; Polypropylene

1. Introduction

Isotactic polypropylene (IPP) has three crystalline phases (α, β, γ) [1–5] and a mesomorphic smectic phase [6]. The chain conformation of each crystalline phase is a 3_1 helix. The polymorphism of polypropylene (PP) is surfacing from different packing of the helix into the unit cell, as observed by wide angle X-ray scattering (WAXS). The α phase always occurs in the regular processed PP as reported by Natta and Corradini [7]. Special crystallization conditions are required [8] to obtain higher amounts of β phase. The γ phase is not enough explored; only recently, its face-centered orthorhombic cell has been clarified [9,10].

The thermal degradation of isotactic polypropylene–carbon nanofibers (IPP–CNFs) is expected to be the result of the superposition of two sigmoids, one representing the thermal degradation of the polymer and the other assigned to the thermal degradation of nanofibers. Due to the absence of oxygen and owing to the high thermal stability of carbon nanofibers in inert atmosphere, only the degradation of the polymer would be sensed by TGA (in the temperature range 50 °C to 1000 °C) [11,12].

2. Experimental techniques

IPP type Marlex HLN-120-01 (Philips Sumika Polypropylene Company) with density 0.906 g/cm^3 and melt flow rate at 230 °C of 12 g/10 min has been utilized as polymeric matrix. Vapor grown carbon nanofibers VGCNFs (PR-24AG) with diameters ranging between 60 and 100 nm and lengths between 30,000 and 100,000 nm have been supplied by Pyrograf Products, Inc and used to reinforce the polymeric matrix, according to the process developed by Lozano and Barrera [13]. In this study purified vapor grown carbon fibers (VGCF) were mixed into the IPP matrix to form nanofiber composites. The purification of VGCNFs implied refluxing VGCNTs in dichloromethane and deionized water followed by vacuum filtering (for 24 h) and drying at 110 °C for at least 24 h. Lozano et al. [14] showed

* Corresponding author. Tel.: +1 956 381 2152; fax: +1 956 381 2423.
E-mail address: mchipara@utpa.edu (M. Chipara).

0141-3910/$ - see front matter © 2008 Elsevier Ltd. All rights reserved.
doi:10.1016/j.polymdegradstab.2008.01.001

that the purification process does not affect the length of VGCNFs.

High-shear mixing has been used to disperse the VGCNFs homogenously throughout the IPP matrix. The mixing has been performed by a HAAKE Rheomix at 180 °C for 9 min with a speed of 65 rpm followed by an additional mixing at 90 rpm for 5 min. Composites loaded with various amounts of VGCNFs (0%, 1%, 2.5%, 5%, 7.5%, 10%, 15%, and 20% wt.) have been prepared.

The as obtained samples have been hot pressed into sheets with a thickness of about 0.6 mm at about 180 °C and at a weight of 9000 kg for 100 s. TGA investigations on the thermal stability of IPP–VGCNF composites in nitrogen, have been performed using a TA Instrument (TGA Q500). Additional data regarding the dispersion of VGCNFs within the polymeric matrix (IPP) have been obtained by using a Philips Transmission Electron Microscope operating at 200 kV.

3. Experimental results and discussions

Fig. 1 shows the temperature dependence of the sample mass for IPP–VGCNFs composites, for different loading concentrations of VGCNFs (ranging from 0% wt. up to 20% wt. VGCNFs). In order to ensure a good reproducibility of experimental data all samples had a weight of about 10.0 ± 1.5 mg. The experimental errors for the as recorded TGA data sets were found to be better than 1%. To observe easily the general trends and the differences between different TGA data sets, all data sets (excepting the one for pristine polymer) have been shifted upwards along the vertical axis by 4 mg relative to the previous data set. The experimental data were not shifted along the horizontal axis.

The temperature dependence of the composite's mass obeys the usual sigmoid like shape [11,12]. The mass evolution as a function of temperature for both the pristine IPP and the IPP–VGCNFs composites is described by single asymmetric sigmoid. From Fig. 1 it is noticed that the thermal degradation of IPP shifts towards higher temperatures as the concentration of VGNCFs is increased. This substantiates the interactions between macromolecular chains and VGCNFs revealing the formation of an IPP–VGCNF interface with enhanced thermal stability. Within the experimental errors, no additional mass loss has been noticed as the temperature of the IPP–VGCNF composites was raised from 700 °C to 1000 °C.

In order to increase the resolution of TGA analysis, the first derivative of the mass loss versus the degradation temperature has been analyzed. The as obtained dependencies are collected in Fig. 2. As in the previous figure, all data sets shown in Fig. 2 were shifted upwards by 0.1 g/°C relative to the previous data set. The data for pristine polymer were not shifted, without any horizontal shift. The dependence of the mass loss derivative versus temperature should present a bell like shape (Lorentzian or Gaussian) as the derivation process converts the inflection point into an extreme point. From Fig. 2 it is

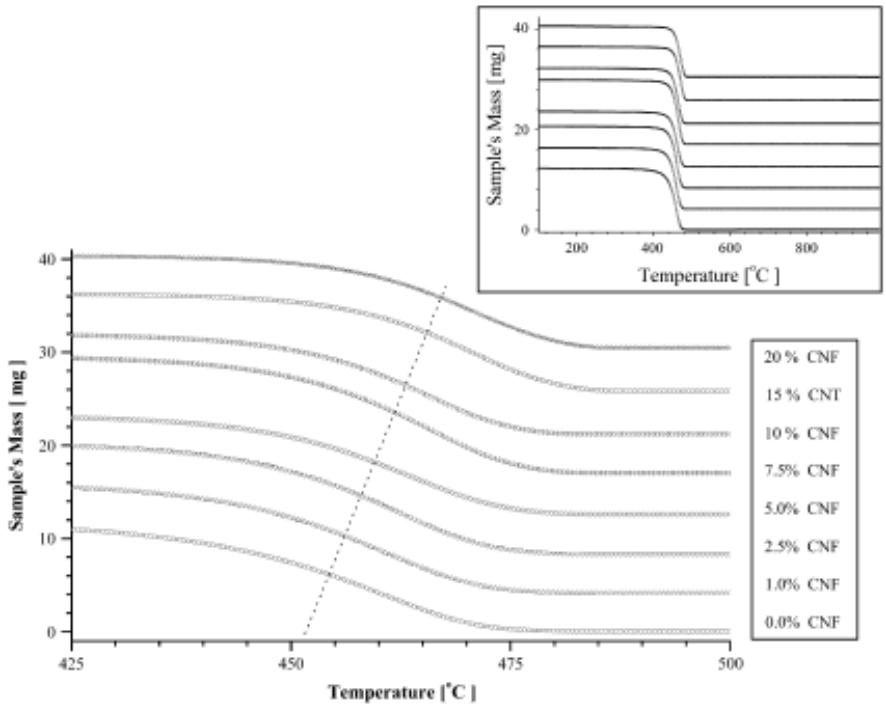

Fig. 1. The temperature dependence of the weight of IPP–VGCNFs composites. The single sigmoidal shape is noticed and the shift of the temperature at which the speed of thermal degradation is maximum as the loading with VGCNFs is increased is emphasized by the dotted line. The inset shows the TGA data for the whole range of temperatures (50 °C–1000 °C). Please notice a vertical offset of 4 mg and no horizontal offset.

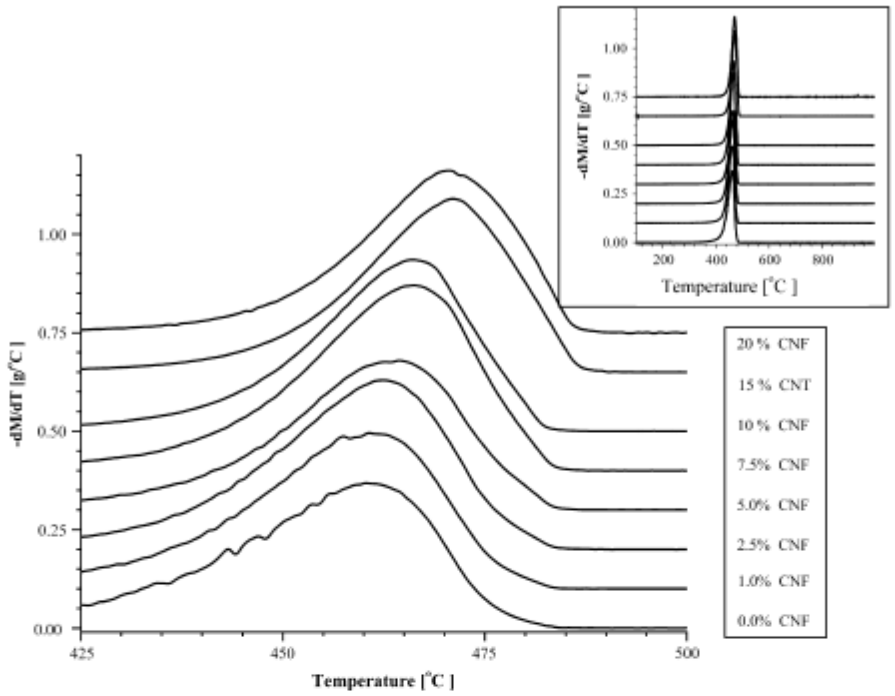

Fig. 2. The dependence of the first derivative of the TGA signal (versus the temperature) on temperature in the degradation region. The inset shows the temperature dependence of the TGA signal for the whole temperature range (50 °C–1000 °C). Please notice a vertical offset of 0.1 g/°C and no horizontal offset.

observed that for all spectra, the derivative of the residual mass (versus the temperature of the sample) as a function of temperature, has a single maximum, is asymmetric, and shifts towards higher temperatures as the concentration of VGCNF is increased. The derivative of the residual mass of the sample as a function of sample temperature has been fitted by an extended Breit Wigner Fano Lorentz line shape:

$$I(\epsilon) = \frac{(P_3 + P_4\epsilon)^2}{P_5\epsilon^2 + P_6} \tag{1}$$

with:

$$\epsilon = \frac{x - P_1}{P_2} \tag{2}$$

where x is the temperature, P_1 defines the temperature at which the mass loss rate is maximum, P_2 identifies the width of the derivative, P_3, P_4, P_5 and P_6 are constants. The simple Lorentzian shape is symmetric and cannot fit accurately the experimental data. The proposed lineshape degenerates into a Lorentzian like line shape for $P_4 = 0$ and $P_5/P_6 = 1$. The Breit Wigner Fano has been frequently used [15–17] in various spectroscopic techniques (such as Raman) to simulate asymmetric resonance lines.

As it is noticed from Fig. 3, the experimental data are fairly well fitted by the proposed line shape. From this equation the maximum of dm/dT, which actually represents the temperature at which the mass loss rate is maximum (named also inflection temperature – T_I), has been estimated. Fig. 4 depicts the dependence of T_I on the concentration of VGCNFs. It is noticed from Fig. 4 that T_I rises as the concentration of VGCNFs dispersed within the polymeric matrix is increased. The dependence of the inflection temperature on the concentration of VGCNFs is well described by the equation:

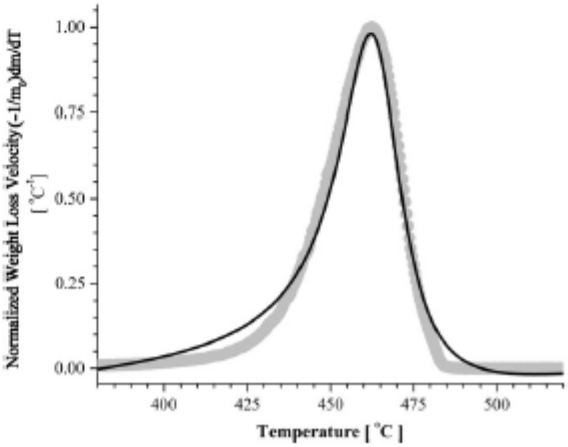

Fig. 3. The first derivative of the sample's mass relative to the sample's temperature as a function of temperature. The black narrow line represents the as recorded data and the gray line the best fit (obtained by using Eq. (1)).

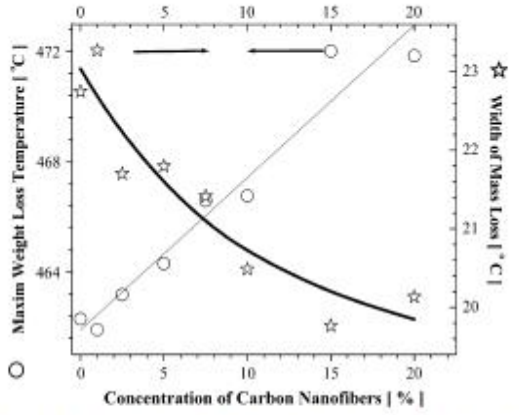

Fig. 4. The effect of the loading with VGCNFs on the temperature at which the thermal degradation is maximum (left axis, open circles). The effect of the loading with VGCNFs on the width of the degradation process (right axis, stars).

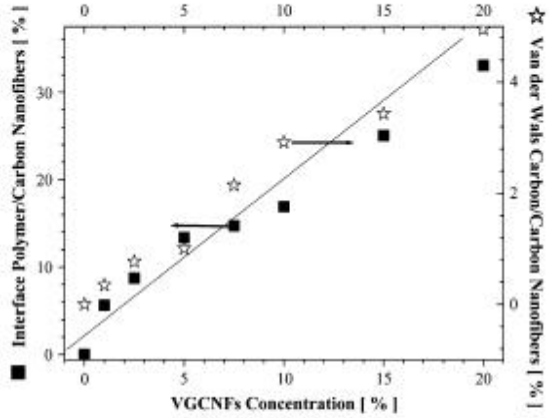

Fig. 5. The dependence of the fraction of polymer chains captured in the elastic layer of the interface on the polymer loading with VGCNFs (left axis, filled squares). The dependence of the fraction of polymer chains (actually mostly C atoms) captured in the hard layer of the interface on the polymer loading with VGCNFs (right axis, stars).

$$T_1 = T_1 + T_2 \exp(Cx) \tag{3}$$

where T_1, T_2, and C are fitting constants and x is the weight fraction of VGCNFs. It is noticed that $T_1 + T_2 = T_1^0$, where T_1^0 is the inflection temperature for the pristine polymer. The experimental data are well fitted by this equation (see the dotted line in Fig. 4). The parameters corresponding to the best fit are $T_1 = -21{,}616 \pm 1$ K, $T_2 = 22{,}078 \pm 1$ K, and $C = 0.00003 \pm 0.00001$. This corresponds to $T_1^0 = 462 \pm 1$ K, which is an acceptable value and confirms the proposed equation (see Fig. 4). The shift of T_1 as the concentration of VGCNFs is increased demonstrates the enhancement of the thermal stability of IPP upon loading with VGCNFs and confirms the formation of IPP–VGCNFs interface. It is this interface that is responsible for the overall increase of the thermal stability of IPP–VGCNFs composites.

The width (calculated between the inflection points of the derivative) of the first derivative of the mass loss (versus temperature) depends on the concentration of VGCNFs (see Fig. 4). It is noticed that the width of the thermal degradation process (W) is narrowed by the loading of the polymeric matrix with CNFs. The dependence of W on the loading with VGCNFs (x) has been fitted by:

$$W = W_1 + W_2 \exp(Dx) \tag{4}$$

where W_1, W_2, and D are fitting constants and $W_1 + W_2$ represents the width of the thermal degradation for the pristine polymer. The dependence of the thermal degradation width on the concentration of VGCNFs is very well described by this equation (see the bold line in Fig. 4). The parameters associated to the best fit are: $W_1 = 19.5 \pm 0.5$ K, $W_2 = 3.5 \pm 0.5$ K, and $D = -0.10 \pm 0.04$. The negative value of D reflects the narrowing of the thermal degradation process as the concentration of VGCNFS dispersed within IPP is increased. TGA data have been utilized to estimate of the mass fraction of the polymer located in the interface, m_{1c}, by using the expression:

$$m_{10} = \frac{m(x)_{10} - m_{10}}{m_{10}} \times 100(\%) \tag{5}$$

where m_{10} is the mass of pristine polymer at the temperature at which the mass loss rate of the pristine temperature is maximum

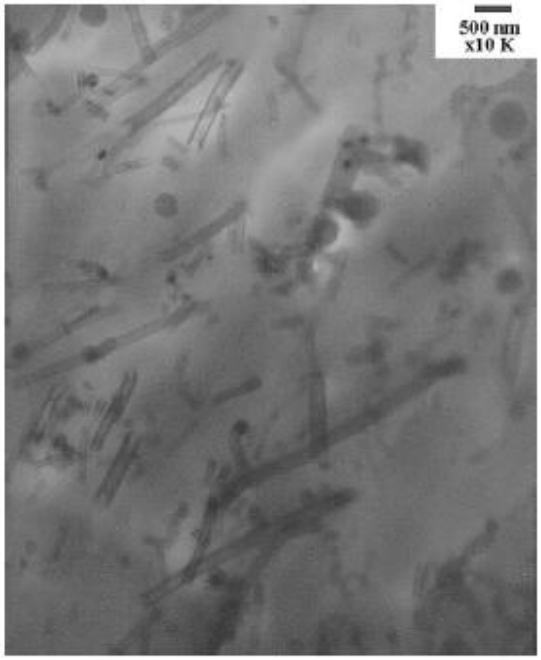

Fig. 6. TEM micrograph of IPP–VGCNF composites loaded with 20% wt. VGCNFs.

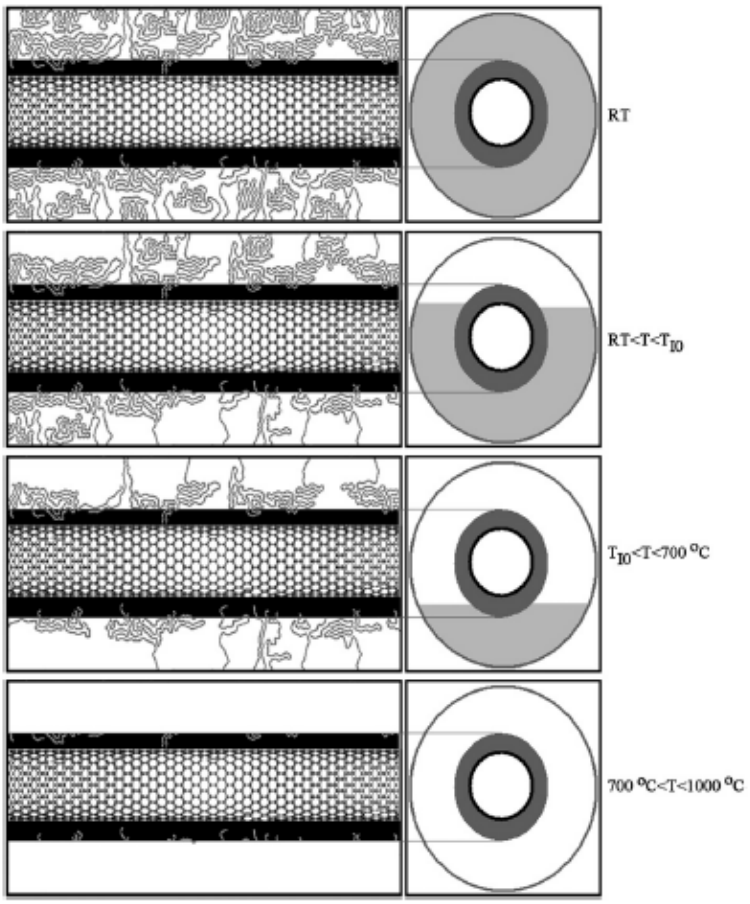

Fig. 7. A model of the adhesion of polypropylene chains to VGCNFs. From the top to bottom, first panel shows the IPP–VGCNFs morphology at room temperature. Second panel shows the morphology of IPP–VGCNFs at temperature lower than the temperature at which the mass loss is maximum (T_{10}). Some macromolecular chains interacting with VGCNFs have been removed due to the enhancement of molecular motions (note that mostly chains that have no molecules in the hard layer were evaporated). Third panel depicts the IPP–VGCNFs immediately above the temperature at which the maximum mass loss is reached. The decrease of the density of macromolecular chains in interaction with VGCNFs is noticed. Last panel shows the VGCNFs above 700 °C. In the temperature range 700 °C–1000 °C the polymer is fully vaporized; only the molecules trapped by strong van der Waals interactions are left on VGCNFs. For such molecules the energy of van der Waals interaction (with the nearest molecules of VGCNFs) is stronger than the energy of the C–C bond. The hard layer is represented by the strong gray color while the light gray color is associated to the elastic layer. The ratio between the light gray and white indicates qualitatively the fraction of polymer confined within the soft layer at a given temperature (relative to RT).

(T_{10}), $m(x)_{10}$ is the mass of the composite containing x% wt. VGCNF that was not degraded at T_{10}. As it is inferred from Eq. (5), the mass fraction (m_{1x}) defines the stability of IPP–VGCNFs. From Fig. 5 it is noticed that m_{1x} increases as the amount of VGCNF dispersed within the IPP is increased. Even more, the dependence of m_{1x} (see Eq. (5)) on the concentration of VGCNFs is almost linear. As the concentration of VGCNFs is proportional to the total contact area between IPP and VGCNFs, Fig. 5 suggests that the thickness of the interface IPP–VGCNFs is not significantly affected by the concentration of VGCNFs. Assuming that the density of VGCNF is about 2 kg/m^3, the polymer density is about 1 kg/m^3, the average diameter of VGCNFs is about 80 nm and the average length 65,000 nm, the thickness of the soft IPP–VGCNFs interface has been estimated to be of the order of 10^2 nm. This value is consistent with the radius of gyration of IPP [18] and indicates that solely the chains that have molecules in contact with the nanofibers have an enhanced thermal stability. This interface is elastic because these segments are not in the near proximity of the CNFs. Hence, these macromolecular chains still preserve a certain degree of flexibility.

A detailed analysis of the residual mass of these composites at fairly large temperatures (above 700 °C) reveals that weight of PP–VGCNFs residues exceeds the weight of VGCNFs. Hence, it is speculated that some carbon atoms originating from the polymer chains wrapped around the nanofibers are

not affected by the thermal treatment. To explain this increase it was assumed that some polymer molecules are captured by VGCNFs via van der Waals interaction. As it is observed from Fig. 5, the fraction of polymer captured by such van der Waals interactions is fairly small and depends linearly on the concentration of VGCNFs. This suggests that these extra carbon atoms scale as the total surface of nanofibers indicating that the thickness of this core layer does not depend significantly on the concentration of VGCNFS in IPP. Actually, the estimated thickness of this extra layer assuming that the density of VGCNFs is 2 kg/m^3 and the polymer density is about 1 kg/m^3 is of the order of 10^0 nm.

In order to fully exploit the benefits derived from the nanometer scale size of VGCNFs it is mandatory to achieve a good dispersion of VGCNFs within IPP. Transmission electron microscopy (TEM) investigations were utilized to check for the dispersion of the nanofiller within the polymeric matrix. As may be noticed from Fig. 6, even for the composite loaded with 20% VGCNFs the filler is well dispersed within the polymeric matrix. This degree of dispersion results in a huge surface area and explains the effect of the interface on the macroscopic thermal stability of the polymeric matrix.

4. Conclusions

The detailed analysis of the thermal degradation of IPP–VGCNFs composites revealed unique and amazing features regarding the morphology and the structure of this nanoreinforced composite (Fig. 7). The observed enhancement of the thermal stability of IPP by the loading with VGCNFs is a direct proof for the existence of an IPP–VGCNFs interface. Mathematical modeling provided quantitative estimations on the inflection temperature shift and suggested a better homogenization of the temperature distribution within the nanocomposite as the loading of VGCNFs is increased.

The experimental data suggested that the IPP–VGCNFs interface has a two-layer structure.

The external or soft layer has a thickness comparable to the radius of gyration of the polymer and contributes to the enhanced thermal stability of the composite. For IPP–VGCNFs this thickness has been estimated to be of the order of 10^2 nm. TGA analysis revealed also a new inner or core layer, with a thickness of the order of 10^0 nm. This layer is tentatively assigned to those molecules belonging to VGCNFs that are located around VGCNFs at distances smaller or equal to 10^0 nm. Such molecules are trapped around VGCNFs molecules by strong van der Waals interactions. These interactions are stronger than the energy of C–C bonds and accordingly during the thermal degradation process the molecules are confined within the core or rigid layer while the polymer degrades and volatilizes. The excellent dispersion of VGCNFs within the polymeric matrix (IPP), confirmed by TEM data, supports the proposed interpretation.

Acknowledgements

This research has been supported by DMR 0606224 and by the US Army STTR grant #A2-1299.

References

[1] Padden FJ, Keith HD. Spherulitic crystallization in polypropylene. J Appl Phys 1959;30(10):1479–84.
[2] Pae KD. γ–α Solid–solid transition of isotactic polypropylene. J Polym Sci Pol Phys 1968;6(4):657–63.
[3] Isasi JR, Mandelkern L, Galante MJ, Alamo RG. The degree of crystallinity of monoclinic isotactic poly(propylene). J Polym Sci Part B Polym Phys 1999;37(4):323–34.
[4] Menyhard A, Varga J, Liber A, Belina G. Polymer blends based on the β-modification of polypropylene. Eur Polym J 2005;4:669–77.
[5] Varga J. Crystallization, melting and supermolecular structure of isotactic polypropylene. In: Karger-Kocsis J, editor. Polypropylene: structure, blends and composites. 1st ed., vol. 1. London: Chapman and Hall; 1995. p. 56–67.
[6] Corradini P, Petraccone C, Rosa CDe, Guerra G. On the structure of the quenched mesomorphic phase of isotactic polypropylene. Macromolecules 1986;19(11):2699–703.
[7] Natta G, Corradini P. Structure and properties of isotactic polypropylene. Nuovo Cimento 1960;15(Suppl):40–51.
[8] Varga J, Ehrenstein GW. Formation of β-modification of isotactic polypropylene in its late stage of crystallization. Polymer 1996; 37(26):5959–63.
[9] Bruckner S, Meille SV. Non-parallel chains in crystalline γ-isotactic polypropylene. Nature (London) 1989;340:455–7.
[10] Lotz B, Wittmann JC, Lovinger AJ. Structure and morphology of poly(propylenes): a molecular analysis. Polymer 1996;37(22):4979–92.
[11] Shen J, Huang W, Wu L, Hu Y, Ye M. Thermo-physical properties of epoxy nanocomposites reinforced with amino-functionalized multi-walled carbon nanotubes. Composites A 2007;38:1331–6.
[12] Zou Y, Feng Y, Wang L, Liu X. Processing and properties of MWNT/HDPE composites. Carbon 2004;42(2):271–7.
[13] Lozano K, Barrera EV. Nanofiber-reinforced thermoplastic composites: thermoanalytical and mechanical analysis. J Appl Polym Sci 2000;79:125–33.
[14] Lozano K, Files B, Rodriguez-Macias F, Barrera EV. Purification and functionalization of vapor grown carbon nanotubes and single wall nanotubes. Symposium powder materials: current research and industrial practices, TSM Fall meeting 1999. p. 333–40.
[15] Brown SDM, Jorio A, Corio P, Dresselhaus MS, Dresselhaus G, Saito R, et al. Origin of the Breit-Wigner-Fano lineshape of the tangential G-band feature of metallic carbon nanotubes. Phys Rev B 2001;63:155414.
[16] Nguyen KT, Gaur A, Shim M. Fano lineshape and phonon softening in single isolated metallic carbon nanotubes. Phys Rev Lett 2007;98:145504.
[17] Banerjee S, Kim DI, Robinson RD, Herman IP, Mao Y, Wong SS. Observation of Fano asymmetry in Raman spectra of $SrTiO_3$ and $Ca_xSr_{1-x}TiO_3$ perovskite nanocubes. Appl Phys Lett 2006;89:223130.
[18] Krause B, Stephan M, Volkland S, Voigt D, Haußler L, Dorschner H. Long-chain branching of polypropylene by electron-beam irradiation in the molten state. J Appl Polym Sci 2006;99:260–5.

BIOGRAPHICAL SKETCH

Anna Alicia Hernandez was born on July 18, 1983 in Weslaco, Texas. She received her Bachelors and Masters of Science in Mechanical Engineering from The University of Texas-Pan American in 2006 and 2013, respectively. She is a great advocate for community involvement and was highly active in her local organizations chapters such as: Society of Women Engineers (SWE) and Society of Hispanic Professional Engineers (SHPE).

In 2005-2006, she was awarded the Minority of Institutions of Excellence Undergraduates Student Research Award while pursuing her undergraduate degree. She served as a Research Assistant in the Department of Mechanical Engineering at The University of Texas- Pan American until 2008, under the supervision of Dr. Karen Lozano.

From 2008-2013, she pursued a career in teaching as a mathematics teacher and became the Co-Department Chair at Johnny G. Economedes High School in Edinburg, Texas. However, in early 2013, she returned to her passion in mechanical engineering to complete her Masters requirements. She obtained an internship and Graduate Engineer I position with the Brownsville Public Utilities Board in 2013.

As of January 2014, she will begin working as a Plastics Reliability Engineer at the DOW Chemical Company in Seadrift, Texas. Ms. Hernandez can be reached at 956-355-8108 or via email ahernandez32@broncs.utpa.edu regarding her career and credentials.